UNIVERSITA' DEGLI STUDI DI VERONA

DEPARTMENT OF

BIOTECHNOLOGY

GRADUATE SCHOOL OF

NATURAL SCIENCE AND ENGINEERING

DOCTORAL PROGRAM IN

NANOSCIENCE AND ADVANCED TECHNOLOGY

CYCLE/YEAR **XXXI/2016**

TITLE OF THE DOCTORAL THESIS

EXPLOITING TRANSITION METAL AND LANTHANIDE IONS AS DOPANTS IN OXIDE AND FULORIDE NANOPARTICLES FOR NANOTHERMOMETRY AND BROAD BAND OPTICAL SENSITIZATION

S.S.D. CHIM/03

Coordinatore: Prof FRANCO TAGLIARO

Firma _____

Tutor: Prof ADOLFO SPEGHINI

Firma _____

Dottorando: Dott. GIACOMO LUCCHINI

Firma _____

Quest'opera è stata rilasciata con licenza Creative Commons Attribuzione – non commerciale Non opere derivate 3.0 Italia . Per leggere una copia della licenza visita il sito web:

http://creativecommons.org/licenses/by-nc-nd/3.0/it/

Attribuzione - Devi riconoscere una menzione di paternità adeguata, fornire un link alla licenza e indicare se sono state effettuate delle modifiche. Puoi fare ciò in qualsiasi maniera ragionevole possibile, ma non con modalità tali da suggerire che il licenziante avalli te o il tuo utilizzo del materiale.

NonCommerciale - Non puoi usare il materiale per scopi commerciali.

Non opere derivate -Se remixi, trasformi il materiale o ti basi su di esso, non puoi distribuire il materiale così modificato.

ESEMPIO:

Exploiting transition metal and lanthanide ions as dopants in oxide or fluoride nanoparticles for nanothermometry and broad band optical sensitization

Giacomo Lucchini

Tesi di Dottorato

Verona, 18 Dicembre 2018

ISBN xxxxx-xxxx-xxx

Abstract

Lanthanide activated nanoparticles are an important class of nanomaterials with unique properties and useful functionalities for a wide range of applications in nanomedicine such as optical imaging, magnetic resonance imaging (MRI), nanothermometry and theranostics. In this thesis some new lanthanide activated, fluoride or oxide nanoparticles for nanomedicine have been investigated. In particular, their synthesis, chemico-physical characterization and spectroscopic properties have been carried out. Two new nanothermometers have been developed through proper lanthanide doping and core@shell architecture, exploiting the peculiar energy level scheme of the lanthanide ions. The obtained nanomaterials show good thermal sensitivity, using both excitation and emission radiation in the near infrared biological windows, suggesting their possible use for *in-vivo* applications. One nanothermometer is based on the upconversion emission of Eu^{3+} ions sensitized by Yb^{3+} and Tm^{3+} ions as dopants in SrF_2 nanoparticles. The other investigated nanothermometer is based on the excitation from thermally excited Stark levels of Nd^{3+} ions present as dopants in KY_3F_{10} nanoparticles.

Cr^{3+} and Yb^{3+} co-doped fluoride and oxide nanoparticles have been synthesized in order to sensitize the Yb^{3+} ions in a wide optical region, exploiting the Cr^{3+} absorption and possible energy transfer to Yb^{3+} ions. Fluoride based $NaSrAlF_6:Cr^{3+}$, Yb^{3+} nanoparticles have been obtained and upon a excitation in the red region (around 650 nm) they show a strong Cr^{3+} emission in the NIR range (around 800 nm) but no Yb^{3+} ions emission was observed. On the other hand, for the $ZnWO_4:Cr^{3+}$, Yb^{3+} nanoparticles, that have been obtained and properly characterized, a strong Yb^{3+} emission around 980 nm is observed on exciting in the absorption range of Cr^{3+} (for this host around 750 nm), due to efficient $Cr^{3+} \rightarrow Yb^{3+}$ energy transfer. The spectroscopic results show that the $ZnWO_4:Cr^{3+}$, Yb^{3+} nanoparticles are good candidates for upconversion emission with broad NIR excitation.

Index

Introduction……..…p. 9

Chapter 1

Engineering efficient upconverting nanothermometers using Eu^{3+} ions …p. 15

1.1 Introduction……p. 15

1.2 Experimental…….. …p. 18

1.3 Results and discussion……p. 20

1.4 Conclusions…….…p. 29

1.5 Bibliography……... …p. 30

Chapter 2

Nd^{3+} activated KY_3F_{10} nanoparticles as nanothermometers based on thermal populated excited state stimulation…… …p. 35

2.1 Introduction……p. 35

2.2 Experimental…….. …p. 37

2.3 Results and discussion……... …p. 39

2.4 Conclusions and perspective .....……. …p. 45

2.5 Bibliography……... …p. 46

Chapter 3

Cr^{3+} sensitization of Yb^{3+} ions for broadband excited upconversion emission…….....…p. 49

3.1 Introduction……p. 49

3.2 Experimental…….. …p. 51

3.3 Results and discussion……... …p. 53

3.4 Conclusions and perspective……. …p. 59

3.5 Bibliography……... …p. 60

Conclusions…….. …p. 63

Acknowledgments…… …p. 65

Introduction

The current large range of applications and the even wider potentials fields of optical devices are the reason why luminescence-based techniques continue to attract the interest of many researches all over the world. Nowadays many materials have been developed, such as fluorescent proteins[1], organic dyes[2], metal complexes[3], semiconductors[4], carbon dots[5], metal nanoparticles[6] and lanthanide-doped inorganic phosphorus[7] for possible use in several applications.

Usual Stokes emission is shown in Scheme 1a, where the emitted photons (green arrow), have lower energy with respect to that of the absorbed photons (blue arrow), because part of their energy is lost in non-radiative processes (black dotted arrow). Some materials have the proprieties to generate anti-Stokes luminescence, that is the emission of photons at higher energy than those used for the excitation radiation. Second-harmonic generation (SHG) and two-photons absorption (TPA) are two kinds of anti-Stokes processes, but they require high peak power, pulsed lasers. On the other hand, upconversion (UC) is an Anti-Stokes process that can be generated with relatively low power continuous wave (CW) lasers or even focused incoherent light,[8] for some particular systems as lanthanide activated materials. The general principle of the UC luminescence can be described in Scheme 1b, in which the

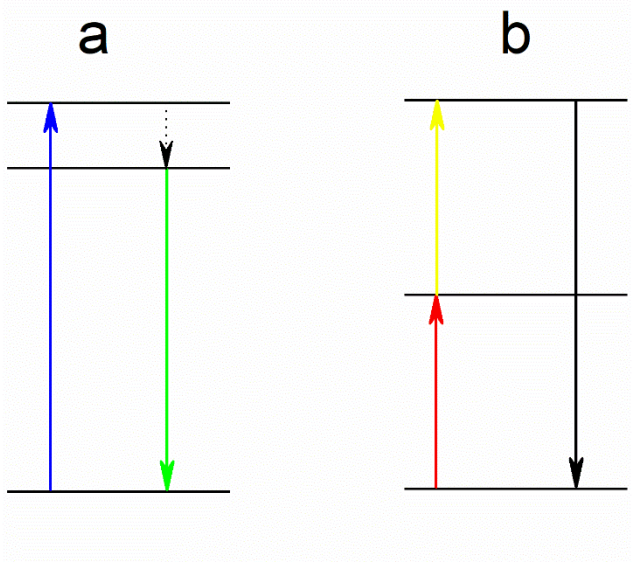

Scheme 1: Schematic principles of a) conventional Stokes emission and b) upconversion luminescence processes.

exciting radiation produce a population of excited levels due to absorption of several photons. As an example, a luminescence center in the ground state can absorb resonantly a photon up to a real level (red line) and subsequently a second photon absorption (yellow line) can populate a higher energy level. Then a radiative transition (black line) from this exited level to the ground state or some other lower energy state allows the emission of photons at higher energy with respect to the excitation radiation. The UC emission is favored if the intermediate excited level has relatively long lifetime. In fact, the lifetime must be long enough to have a sufficient population in the intermediated excited state to allow the transition to the final excited state taking place. To date, two main processes have been found capable of UC luminescence: the so-called triplet-triplet annihilation,[9] that take advantages of the long lifetime of triplet state typical of phosphorescence, and the UC emission due to lanthanide ions.

Since the pioneering work of Auzel and co. on the Er^{3+} UC luminescence by pumping Yb^{3+} in a glass matrix in the 1960s, many UC materials have been reported.[10] Most of them are based on the incorporation of lanthanide ions as sensitizers and emitters because of the 4f-electron configurations of these ions have several energy levels with long lifetimes (in the order of microseconds or even milliseconds). Lanthanide-doped materials have interesting luminescence properties including large Stokes or Anti-Stokes shifts (even of several hundred meV), high photostability, sharp emission lines and long lifetimes. These materials were studied in bulk inorganic hosts and found applications in laser technology, anticounterfeiting and optical devices.[10–12]

In the last 20 years, the focus of many researches has been on the development of lanthanide based UC materials at the nanoscale.[13] Many results have been achieved on the control of size, structure, morphology, surface ligands as well as on the luminescence properties of upconverting nanomaterials. The possibility of synthesized such nanostructures pave the way to many fields of applications such as optical bioimaging of living cells[14] and small animals,[15] biosensors,[16] chemosenosors[17] and other optical fields.[18]

In this thesis, some potential applications of lanthanide doped nanoparticles are shown, in particular in Nanomedicine. In 2011 our group presented a one-pot hydrothermal synthesis of citrate-capped, water dispersible upconverting CaF_2 nanoparticles, doped with Yb^{3+} and Tm^{3+} ions, suggesting that these materials could be used for biomedical applications.[19] This methodology of the synthesis can be used to prepared similar hosts as SrF_2 or ternary fluorides, as $NaYF_4$ or KY_3F_{10}. These materials can be easily doped with trivalent lanthanide ions, because the similarity of the ionic radius between Sr^{2+} and Y^{3+} and the doping lanthanide ions, as Yb^{3+}, Er^{3+}, Tm^{3+} or Ho^{3+}.

The firsts two chapters of this thesis will focus on the development of lanthanide doped nanothermometers. Optical nanothermometry is a field that is rapidly growing and that could have important scientific, diagnostic and therapeutic applications.[20] On the scientific side, the measure of the temperature *in vitro* and *in vivo* of biological systems with high spatial and thermal resolution is of great interest: even slightly elevated temperatures can shift the balance between proper assembly and disassembly of cell structures, leading to alterations in cell morphology and functioning.[21] The measure of temperature can be important also as a diagnostic tool. As an example, has been proved that the thermal relaxation of a tissue after subjecting it to a slightly heating or cooling could give important information about the physiological state of the tissue. Recently it has been demonstrated in mice that is possible to have an early detection and diagnosis of tumors thanks to nanothermometry.[22]

Finally, on the therapeutic side, nanothermometers can be used as tools for cancer therapies. In particular, some NIR absorbing nanoparticles such gold nanoparticles or Nd^{3+} doped nanoparticles, have shown interesting abilities to perform thermal treatment of tumors, when they are illuminated with strong NIR light.[23] During a thermal treatment the local temperature can easily exceed the safety threshold for the therapy, since the temperature level must be high enough to kill cancer cells without harming the healthy cells. Nanothermometers could be a useful tool to instantaneously monitor the local temperature, avoiding overheating.[24]

From a general point of view to perform a thermometric measurement, we need a measurable quantity that changes when the temperature changes, e.g. in the old mercury thermometers the level of mercury used to change with temperature, or in modern electronic thermometers a change in the conductivity is measured, etc.

In the case of optical nanothermometers, one of the most useful parameters that can be measured are variations in the nanoparticles emission intensity when temperature changes.[25] Many strategies have been developed to achieve a high thermometric performance with nanoparticles, some of them rely on single nanoparticles, while others use more complicated hybrid structures, combining lanthanide doped nanoparticles with quantum dots, or functionalizing the nanoparticles with fluorescent molecules.[26,27]

In the first chapter of this thesis, we develop a new kind of nanothermometers thanks to the engineering of nanoparticles with three different lanthanide ions (Yb^{3+}, Tm^{3+} and Eu^{3+}). The nanothermometers produce in this way have shown good sensibility and is unaffected by the excitation power, being a good candidate for an actual application.

In the second chapter, we develop a double nanothermometer that works simultaneously both in ordinary Stokes and UC emission. This nanothermometer is based on a recent proposed mechanism of absorption from thermally excited level of the ground state.[28] We exploit the thermometric properties of Nd^{3+} doped nanoparticles of KY_3F_{10} excited from the ground level and from an excited Stark level.

In the last chapter we explore the possibility to enhance the UC emission through the sensitization of lanthanide ions with transition metal ones, in particular with Cr^{3+} ions, which have much higher and broader absorption cross section. The preliminary results show that it is possible to synthesize nanocrystalline structures co-doped with Cr^{3+} ions and Yb^{3+}, but that the sensitization of the last one is strongly dependent on the crystal field and the phonon distribution of the host material.

Bibliography

1. Schneider, A. F. L. & Hackenberger, C. P. R. Fluorescent labelling in living cells. *Curr. Opin. Biotechnol.* **48,** 61–68 (2017).
2. Hara, K. & Mori, S. Dye-sensitized Solar Cells. 6595–6663 (2011).
3. Ye, B. H., Tong, M. L. & Chen, X. M. Metal-organic molecular architectures with 2,2′-bipyridyl-like and carboxylate ligands. *Coord. Chem. Rev.* **249,** 545–565 (2005).
4. Dai, X. *et al.* Solution-processed, high-performance light-emitting diodes based on quantum dots. *Nature* **515,** 96–99 (2014).
5. Lim, S. Y., Shen, W. & Gao, Z. Carbon quantum dots and their applications. *Chem. Soc. Rev.* **44,** 362–381 (2015).
6. Cui, M., Zhao, Y. & Song, Q. Synthesis, optical properties and applications of ultra-small luminescent gold nanoclusters. *TrAC - Trends Anal. Chem.* **57,** 73–82 (2014).
7. Zhou, J., Liu, Q., Feng, W., Sun, Y. & Li, F. Upconversion luminescent materials: Advances and applications. *Chem. Rev.* **115,** 395–465 (2015).
8. Chen, G. *et al.* Energy-Cascaded Upconversion in an Organic Dye-Sensitized Core/Shell Fluoride Nanocrystal. *Nano Lett.* **15,** 7400–7407 (2015).
9. Ceroni, P. Energy up-conversion by low-power excitation: New applications of an old concept. *Chem. - A Eur. J.* **17,** 9560–9564 (2011).
10. Auzel, F. Upconversion and Anti-Stokes Processes with f and d Ions in Solids. *Chem. Rev.* **104,** 139–173 (2004).
11. Scheps, R. Upconversion laser processes. *Prog. Quantum Electron.* **20,** 271–358 (1996).
12. Gamelin, D. R. & Gudel, H. U. Upconversion Processes in Transition Metal and Rare Earth Metal Systems BT - Transition Metal and Rare Earth Compounds: Excited States, Transitions, Interactions II. in (ed. Yersin, H.) 1–56 (Springer Berlin Heidelberg, 2001). doi:10.1007/3-540-44474-2_1
13. Ang, L. Y., Lim, M. E., Ong, L. C. & Zhang, Y. Applications of upconversion nanoparticles in imaging, detection and therapy. *Nanomedicine Nanotechnology, Biol. Med.* **6,** 1273–1288 (2011).
14. Lingeshwar Reddy, K. *et al.* Core-Shell Structures of Upconversion Nanocrystals Coated with Silica for Near Infrared Light Enabled Optical Imaging of Cancer Cells. *Micromachines* **9,** 400 (2018).
15. Cheng, L. *et al.* Highly-sensitive multiplexed in vivo imaging using pegylated upconversion nanoparticles. *Nano Res.* **3,** 722–732 (2010).

16. Wang, L. *et al.* Fluorescence resonant energy transfer biosensor based on upconversion-luminescent nanoparticles. *Angew. Chemie - Int. Ed.* **44,** 6054–6057 (2005).
17. Li, J., Yang, C., Wu, Y., Zhu, R. & Zhao, K. The combination of rare earth upconversion nanocrystals with rhodamine dyes for the selective detection of amino acids. *J. Lumin.* **204,** 195–202 (2018).
18. González-Béjar, M. & Pérez-Prieto, J. Upconversion luminescent nanoparticles in physical sensing and in monitoring physical processes in biological samples. *Methods Appl. Fluoresc.* **3,** 42002 (2015).
19. Dong, N. N. *et al.* NIR-to-NIR two-photon excited CaF2:Tm3+,Yb3+nanoparticles: Multifunctional nanoprobes for highly penetrating fluorescence bio-imaging. *ACS Nano* **5,** 8665–8671 (2011).
20. Rosal, B., Ximendes, E., Rocha, U. & Jaque, D. In Vivo Luminescence Nanothermometry : from Materials to Applications. *Adv. Opt. Mater.* **5,** 1600508 (2017).
21. Repasky, E. A., Evans, S. S. & Dewhirst, M. W. Temperature Matters! And Why It Should Matter to Tumor Immunologists. *Cancer Immunol. Res.* **1,** 210–216 (2013).
22. Santos, H. D. A. *et al.* In Vivo Early Tumor Detection and Diagnosis by Infrared Luminescence Transient Nanothermometry. *Adv. Funct. Mater.* **1803924,** 1–10 (2018).
23. Chen, J. *et al.* Nanomaterials as photothermal therapeutic agents. *Prog. Mater. Sci.* **99,** 1–26 (2019).
24. Quintanilla, M. & Liz-Marzán, L. M. Guiding Rules for Selecting a Nanothermometer. *Nano Today* **19,** 126–145 (2018).
25. Jaque, D. & Vetrone, F. Luminescence nanothermometry. *Nanoscale* **4,** 4301–4326 (2012).
26. Cerõn, E. N. *et al.* Hybrid Nanostructures for High-Sensitivity Luminescence Nanothermometry in the Second Biological Window. *Adv. Mater.* **27,** 4781–4787 (2015).
27. Donner, J. S., Thompson, S. A., Kreuzer, M. P., Baffou, G. & Quidant, R. Mapping intracellular temperature using green fluorescent protein. *Nano Lett.* **12,** 2107–2111 (2012).
28. Souza, A. S. *et al.* Highly-sensitive Eu^{3+} ratiometric thermometers based on excited state absorption with predictable calibration. *Nanoscale* **8,** 5327–5333 (2016).

Chapter 1

Engineering efficient upconverting nanothermometers using Eu^{3+} ions

1. Introduction

The development of all-optical nanoparticle-based thermometers allows for the measurement of localized temperature with high spatial resolution in sub-millimeter areas, which serves as a tool for the characterization of microfluidic channels or electronic microcircuit surfaces .[1–3] Particularly interesting are the optical luminescent nanothermometers, that, once excited in their absorption region, exhibit a temperature-dependent emission, usually in the ultraviolet (UV) visible or near infrared (NIR) region . Several magnitudes related to the emission properties can serve as thermal probes, such as intensity, intensity ratios, bandwidth, luminescence lifetimes or band shifts.[4–6] However, not all of them are equally advantageous when it comes to real applications. For instance, using the intensity of a single emission band can be misleading if the concentration of nanoparticles in the area under investigation is not well controlled, since it can create intensity fluctuations not related to temperature but to a different number of emitters. For this reason, it is a good option to analyze parameters that are independent on the concentration of the nanoparticles, as it is the case of luminescence lifetimes, bandwidths, band intensity ratios or peak shifts.[3] However, from the implementation point of view, the measurement of light intensity presents the advantage of less complex optical setups than for lifetimes measurements, and often have higher sensitivities than bandwidth or peak shifts measurements. In the present investigation, a ratiometric technique was proposed to evaluate the temperature[5], where the intensity of an emission band is used as reference for a different, separate band, to avoid the mentioned concentration-triggered uncertainty. This luminescence intensity ratio (LIR), offers a further point of reliability also by removing any inaccuracy caused by uncontrolled fluctuations

of the excitation light. LIRs are often exploited for lanthanide (Ln^{3+}) based nanothermometers, where several thermally-coupled pairs of states have been already investigated and reported in the literature.[7] The emission bands of Ln^{3+} ions are typically narrow and well defined and this feature permits to restrict the range in which the emission spectra need to be measured to estimate temperature values. Besides, narrow emission bands facilitate the option of multiplexing, if more than one probe has to be used.

The upconversion (UC) properties shown by several Ln^{3+} ions, i.e. to generate photons at higher energies with respect to the excitation radiation, are due to the unique ladder-like arrangement of their 4*f* energy level states, coupled with the relatively long lifetimes of these levels, typically in the microseconds or even milliseconds timescale[8,9]. UC has interesting advantages with respect to the usual Stokes emission in the visible range. In fact, the excitation radiation can be chosen in the NIR range, where common solvents, such as water, are poorly absorbing and heat transfer to the sample from the excitation radiation is minimized. Second, UC processes are multiphoton in nature and therefore they permit a higher spatial resolution due to the non-linear dependence of the emission on the power density of the exciting radiation. Third, since the excitation and emission radiation are well separated in energy, the emitted radiation can be easily isolated from the exciting radiation. This avoids any interference into the detection system, and therefore provides excellent signal to noise ratio, which is further supported by the lack of autofluorescence from additional molecules that might be present in the environment.[10]

One of the most studied upconverting Ln^{3+} based system for LIR nanothermometry involves Er^{3+} ions co-doped with Yb^{3+} ones, to enhance the harvesting of the excitation light in the NIR region (around 980 nm).[4,7,11] However, previous studies with different materials have demonstrated that alternative Ln^{3+} ions, such as Dy^{3+} ions[12–14], Eu^{3+} ions[15,16] or Pr^{3+} ions[17,18], can show better thermal sensitivities, although they are less efficiently excited through upconversion processes.[19] Among these ions, Eu^{3+} is a particularly interesting luminescent probe in fields such a biomedicine[20], luminescent inks for anti-

counterfeiting[21] as well as thermometry[22]. However, the Eu^{3+} energy level structure does not permit UC emission by directly exciting with NIR radiation in the biological windows (700-1200 nm), due to lack of resonant energy levels. Nonetheless, with a proper codoping with Yb^{3+} ions, that are sensitizers of NIR excitation radiation at 980 nm, the Eu^{3+} ions can show UC in the red region in the visible[23]. A population of the excited states of the Eu^{3+} ions can be obtained through a simultaneous energy transfer from two different Yb^{3+} ions to an Eu^{3+} ion, a cooperative process that has relatively low probability.[24,25] On the other hand, other Ln^{3+} ions, for instance Tm^{3+}, with energy levels resonant with those of Eu^{3+}, could help in populating Eu^{3+} levels through energy transfer processes and therefore dramatically improve UC emission.[26,27] Following these considerations, with the target of exploiting Eu^{3+} ions UC for nanothermometry while allowing for NIR excitation, we chose a triple doping strategy (Yb^{3+}, Tm^{3+}, Eu^{3+}), implemented in water dispersible SrF_2 nanoparticles in colloidal form, which have been shown to be excellent hosts for UC luminescence, easily prepared in particle sizes as small as 15 nm.[28]

2. Experimental

2.1 Nanoparticles Preparation

Tm^{3+}, Yb^{3+} and Eu^{3+} tridoped SrF_2 upconverting nanoparticles (UCNPs) were synthesized following a hydrothermal method.[29] Briefly, $SrCl_2{\cdot}6H_2O$, $YbCl_3{\cdot}6H_2O$, $TmCl_3{\cdot}6H_2O$ and $EuCl_3{\cdot}6H_2O$ (Aldrich, 99.9%) were used as metal precursors (with Sr^{2+}:Yb^{3+}:Eu^{3+}:Tm^{3+} = 0.745:0.220:0.030:0.005 nominal molar ratios). As a reference sample, Yb^{3+} and Eu^{3+} codoped SrF_2 nanoparticles (with Sr^{2+}:Yb^{3+}:Eu^{3+}=0.750:0.220:0.030 nominal molar ratios) were synthesized following the same procedure and are denoted as SrF_2:Yb,Eu nanoparticles. Stoichiometric amounts of the metal chlorides (3.5 mmol of total metal ions) were dissolved in 7 mL of deionized water. This solution was then added to 25 mL of a 0.8 M sodium citrate dihydrate solution (Fluka, > 99%) and 3.0 mL of a 3.5 M NH_4F solution (Aldrich, 99.9%). The obtained solution was heat treated at 190 ^oC for 6 hours in a stainless-steel Teflon lined digestion pressure vessel (DAB-2, Berghof). Subsequently, the UCNPs were precipitated with acetone and directly dispersed in deionized water. The colloidal dispersion is stable for at least one month.

2.2 Experimental setup

2.2.1 Structural and morphological investigation

X-ray power diffraction (XRPD) measurements were carried out with a Thermo ARL X'TRA powder diffractometer equipped with a Cu-anode X-ray source with a Peltier Si(Li) cooled solid state detector. Before the measurements, the samples were homogenized in a mortar with few drops of ethanol. After evaporation of the ethanol, the sample was deposited on a low background sample stage.

TEM (HRTEM) images were measured using a JEOL 3010 high resolution electron microscope (0.17 nm point-to-point resolution at Scherzer defocus), operating at 300 kV, equipped with a Gatan slow-scan CCD camera (model 794) and an Oxford Instrument EDS microanalysis detector (Model 6636).

The powders were dispersed in water in order to be deposited on Holey-Carbon Copper grids.

2.2.2 Spectroscopy measurements

Emission spectra (spectral resolution of 5 cm^{-1}) were measured using a 980 nm laser diode (MDLIII980, CNI) as the excitation source, a half meter monochromator (Sr-500i, ANDOR) equipped with a CCD camera (DU420A-BVF, ANDOR) as the recording setup. Emission spectra at different temperatures were recorded by heating the solution with a thermal bath and measuring the temperature with a K-type thermocouple (0.2° C sensitivity).

3. Results and discussion

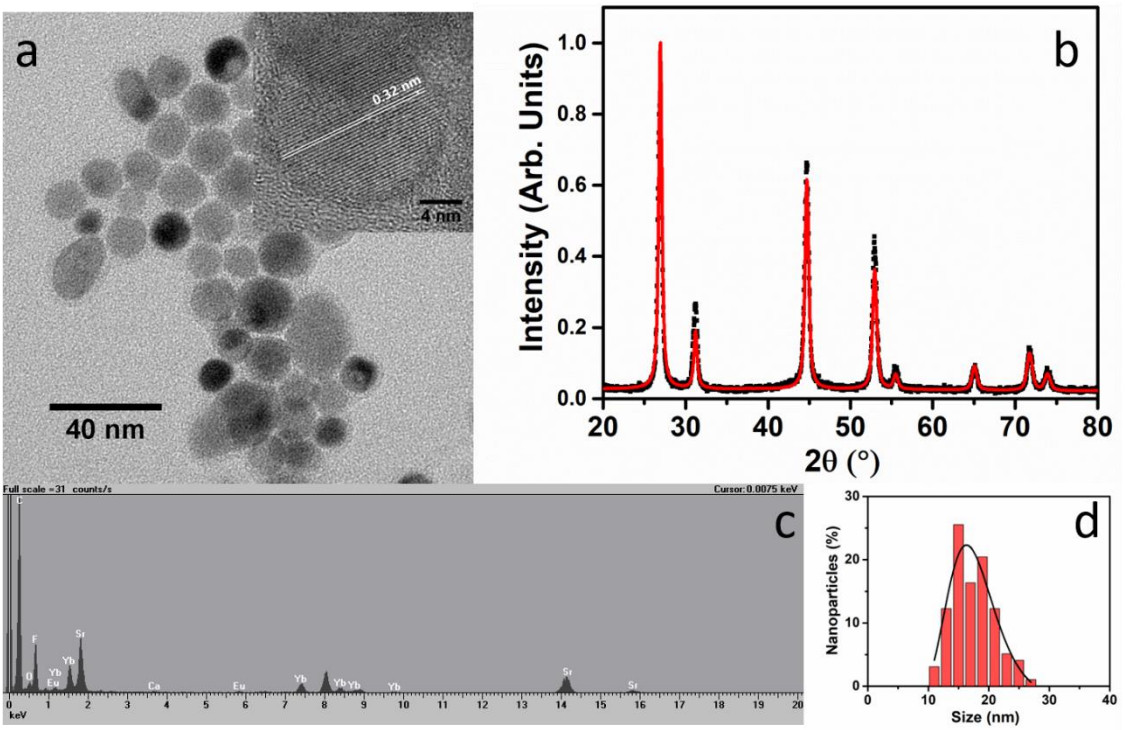

Figure 1. (a) Representative TEM image for the SrF_2:Yb^{3+}, Tm^{3+}, Eu^{3+} UCNPs. Inset: HRTEM image, showing the (111) lattice planes. (b) XRPD pattern of SrF_2:Yb^{3+}, Tm^{3+}, Eu^{3+} UCNPs (black squares). Rietveld refinement, using MAUD software (red line) (lattice parameter: 5.734 ± 0.002). (c) EDX spectra for the SrF_2:Yb^{3+},Tm^{3+},Eu^{3+} UCNPs. (d) Particle size distribution calculated using Pebbles software and Log-normal fit (average particle size: 16 ± 4 nm).

The X-ray diffraction pattern (shown in Figure 1b) show that the prepared UCNPs have a cubic fluorite phase, as reported for similar nanoparticles[28]. EDX measurements clearly indicate the presence of Yb^{3+} and Eu^{3+}, while Tm^{3+} ions are present in concentration below the limit of detection of the EDX setup (Figure 1c). Nonetheless, the presence of Tm^{3+} ions is clearly demonstrated by the strong UC emission, see below. A representative TEM micrograph of the UCNPs is shown in Figure 1a, presenting a nice dispersion and average particle size of 16 nm (see Figure 1d).

Upon laser excitation at 980 nm, a large number of emission bands in the near ultraviolet, blue and red optical regions are observed for the SrF_2:Yb^{3+},Tm^{3+},Eu^{3+} UCNPs[28,30–32] as shown in Figure 2. After 980 nm laser

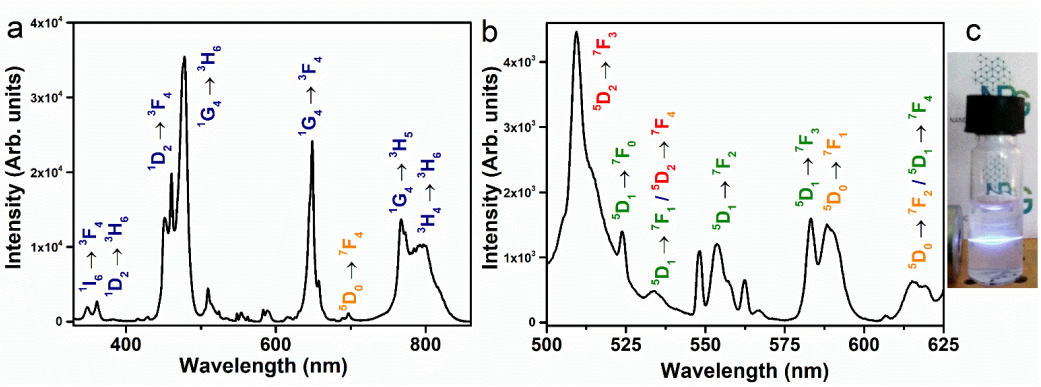

Figure 2. (a) Upconversion emission of a water colloidal dispersion of the SrF_2:Yb^{3+}, Tm^{3+}, Eu^{3+} UCNPs (1 wt %, dopant percentage: Yb^{3+} 22%, Tm^{3+} 0.5%, Eu^{3+} 3%) after laser excitation at 980 nm (power density of 450 mW/mm^2). (b) same as (a) in the 500-650 nm range (dark red frame). Blue: Tm^{3+} ions transitions. Orange: Eu^{3+} ions transitions from the $^5D_0$ level. Green: Eu^{3+} ions transitions from the $^5D_1$ level. Red: Eu^{3+} ions transition from the $^5D_2$ level. (c) Picture of D_2O colloidal dispersions of the SrF_2:Yb^{3+}, Tm^{3+}, Eu^{3+} UCNPs (concentration of 1 wt %) after laser excitation at 980 nm (power density of 450 mW/mm^2).

excitation, several Tm^{3+} excited states can be populated following energy transfer processes from Yb^{3+} to Tm^{3+} ions, as described by the grey dashed arrows in Figure 3a. Several emission bands are thus related to transitions from different Tm^{3+} excited states either to the ground state ($^3H_6$) or to lower lying excited states (see blue labels in Figure 2).

In addition, a group of less intense bands in the 400-440 nm and 500-630 nm regions are nicely observed, as shown in Figure 2b, typical of emission of Eu^{3+} ions, which constitutes clear evidence of population of excited energy levels of Eu^{3+} ions through upconversion processes. The transition assignments for the observed bands have been carried out considering the spectroscopic investigation of Jouart et al. [33] and Cortelletti et al. [39] for Eu^{3+} centres in SrF_2 using site-selective excitation techniques.

In principle, an $Yb^{3+} \rightarrow Eu^{3+}$ cooperative upconversion process could be present[23,34–36]. Nonetheless, the SrF_2:Yb,Eu NPs, prepared as a reference, without Tm^{3+} ions, do not show any Eu^{3+} upconversion emission upon 980 nm laser excitation in the same experimental conditions. Therefore, the Eu^{3+} upconversion emission found for the tridoped SrF_2:Yb^{3+},Tm^{3+},Eu^{3+} NPs clearly

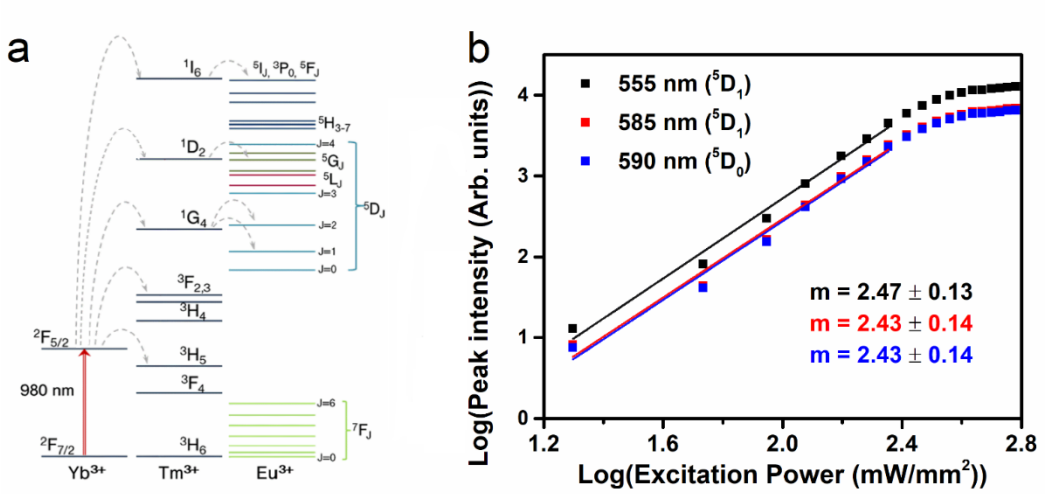

Figure 3. (a) Energy level scheme for Yb^{3+}, Tm^{3+} and Eu^{3+} ions, Yb^{3+} excitation (red arrow) and energy transfer processes (grey dashed arrows). (b) power study for several Eu^{3+} upconversion bands of the SrF_2:Yb^{3+}, Tm^{3+}, Eu^{3+} UCNPs upon 980 nm laser excitation at 25 °C.

indicates that a Tm^{3+}→Eu^{3+} energy transfer is involved and it is active once the excited levels of Tm^{3+} ions have been populated by the Yb^{3+}→Tm^{3+} upconversion. The population of the Eu^{3+} energy levels by means of excited Tm^{3+} ions is already reported in the literature[37,38]. From an inspection of the energy levels of the Tm^{3+} ions, energy transfer processes responsible of the Eu^{3+} energy levels population are sketched in Figure 3. It is interesting to note that the Eu^{3+} emission bands shown in the upconversion spectra (see Figure 2b) have very different relative intensities than those observed in Stokes Eu^{3+} emission spectra for SrF_2:Eu^{3+} nanoparticles upon direct excitation of the Eu^{3+} excited energy levels, as reported by Cortelletti et al. [39]. This different behavior can be explained considering the different pathways populating the Eu^{3+} excited levels, that in the present case are feed through Tm^{3+} → Eu^{3+} energy transfer processes. A similar Tm^{3+} to Eu^{3+} energy transfer process has been also observed for tridoped Eu,Tm,Yb lithium lanthanide phosphate nanoparticles, after excitation at 975 nm with a diode laser.[27]

Some weak emission bands observed in the blue region around 415 and 430 nm, correspond to emissions from the $^5D_3$ level of the Eu^{3+} ions, indicating that an energy transfer process from the $^1D_2$ level of Tm^{3+} to the $^5D_4$, ^5G_J

or ^5L_J levels of Eu^{3+} is present. A contribution to the population of the Eu^{3+} excited levels could be in principle also due to an energy transfer process from the $^1I_6$ level of Tm^{3+}, as emission from this level is observed in the UC spectrum (see Figure 2). Nonetheless, it is reasonable to consider this contribution as much less relevant with respect to those due to energy transfer starting from the lower lying $^1D_2$ and $^1G_4$ excited energy levels of Tm^{3+} ions. This behavior is due to the much lower population of the $^1I_6$ level with respect to the other two levels, evidenced by the very low relative intensity of the $^1I_6 \rightarrow {}^3F_4$ band (see Figure 2a). Moreover, the energy of the $^1G_4$ level of Tm^{3+} ions is slightly higher than the $^5D_1$ level of Eu^{3+} ions, thus a $Tm^{3+}(^1G_4) \rightarrow Eu^{3+}(^5D_1)$ energy transfer process is reasonably present, with possible phonon emission. A $Tm^{3+}(^1G_4) \rightarrow Eu^{3+}(^5D_2)$ energy transfer process can be also possible considering that the $Tm^{3+}(^1G_4)$ and $Eu^{3+}(^5D_2)$ levels are almost resonant, with small phonon absorption assistance.

The upconversion mechanisms described in Figure 3a therefore play a fundamental role to populate the Eu^{3+} energy levels. In order to investigate the power dependence of the Eu^{3+} upconverted luminescence, UC spectra were measured as a function of the 980 nm laser power density (between 20 and 500 mW/mm^2) and they are shown in Figure3b. The peak intensities for the different transitions follow a log-log behavior for laser powers up to ~190 mW/mm^2, and then a saturation behavior is reached. The slopes, denoted as *m*, associated to each transition were evaluated in the linear regime, as they are related to the number of photons involved in the upconversion process. The *m* values are much higher than 2, indicating that a three-photon process is present, and therefore suggesting that the population of the Eu^{3+} energy levels mainly derive from energy transfer from the $^1G_4$ level of Tm^{3+} ion. We point out that the Eu^{3+} upconversion is observable with our experimental setup for laser powers (at 980 nm) as low as 20 mW/mm^2 (2 W/cm^2), value that is comparable with those employed to generate upconversion for similar water dispersed nanoparticles[39]. It is important to note that as transitions starting from $^5D_2$, $^5D_1$ and $^5D_0$ energy levels of Eu^{3+} show the same power dependency, any intensity ratio between emissions originating from these levels

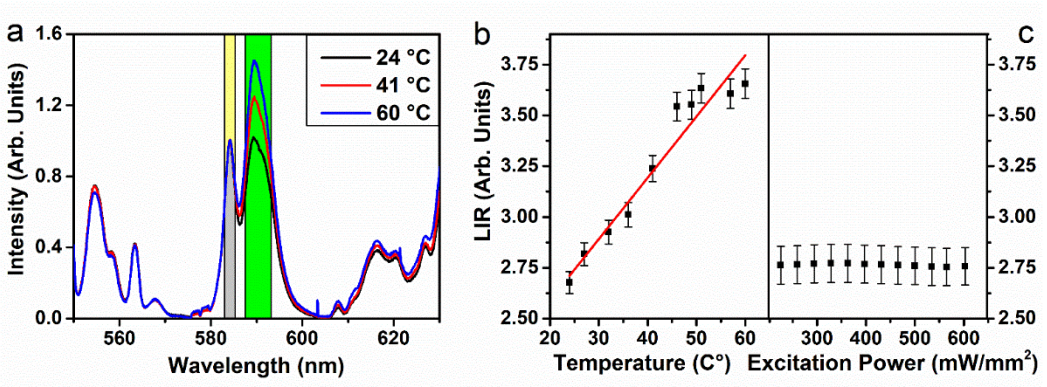

Figure 4 (a) Emission spectra of the SrF_2:Yb^{3+}, Tm^{3+}, Eu^{3+} UCNPs at three different temperatures (intensity normalized to the 585 nm band) upon 980 nm excitation. (b) Luminescence intensity ratio, LIR = $A(^5D_0 \rightarrow {}^7F_1)/A(^5D_1 \rightarrow {}^7F_3)$ vs T. (c) LIR vs laser excitation power.

is independent of the excitation power, a paramount property for a reliable luminescence thermometric system. The non-radiative relaxation probability of the ^5D_J (J=0, 1, 2) levels is in principle different, due to the different energy gaps between each level and the next lying one,[28,40] and therefore the relative intensities of the emission bands could vary on changing the temperature. In addition, the energy transfer mechanisms from $^1G_4$ (Tm^{3+}) to the $^5D_1$ (Eu^{3+}) is non-resonant (see Figure 3) and thus, dependent on the phonon density of states. The UC spectra for the SrF_2:Yb^{3+}, Tm^{3+},Eu^{3+} UCNPs were measured as a function of the temperature in the 20-60 °C range. Representative examples are shown in Figure 4a, from which it can be noted that the Eu^{3+} emission bands in the 580-600 nm range show a notable relative variation on changing the temperature. We define the LIR as:

$$\mathbf{LIR} = \frac{A(\,^5D_0 \rightarrow {}^7F_1)}{A(\,^5D_1 \rightarrow {}^7F_3)} \qquad (1)$$

where *A* denotes an integrated emission of the corresponding transition, as evidenced by shaded areas in Figure 4a. As shown in Figure 4b, the LIR shows a monotonic increasing behavior on increasing the temperature in the investigated range (20-60 °C). In order to evaluate possible variations of the LIR with the laser excitation power, we have measured a series of upconversion spectra at increasing power densities, and the results are shown in Figure 4c. Very importantly, from these results we demonstrate that the LIR value is

independent on the laser excitation power in the range 200-600 mW/mm^2 (see Figure 4c). From the Eu^{3+} upconversion bands (shown in Figure 2), it can be deduced that the $^5D_1$ and $^5D_0$ states are separated by an energy gap around 1800 cm^{-1}, a value consistent with that found for SrF_2:Eu^{3+} based samples on site-selective spectroscopy.[33,41] The fact that the LIR shows a growing trend on increasing the temperature and not a decreasing one indicates that the $^5D_1$ and $^5D_0$ states are not thermally linked, but their population depends by the $Tm^{3+}\rightarrow Eu^{3+}$ energy transfer process, shown in Figure 3a, and subsequent non-radiative processes. The relative sensitivity, S_r, of a thermometer, a commonly accepted parameter to compare the performances of different thermometers[4], is defined as:

$$\boldsymbol{S_r = \frac{1}{LIR}\left(\frac{\partial LIR}{\partial T}\right)} \quad (2)$$

The S_r values as a function of the temperature are shown in Figure 5 and are determined to be between 0.8 and 1.1 %K^{-1} in the 20-60 °C temperature range, with a percentage error of 5%. These values are among the highest reported in the literature for upconverting nanothermometers, as reported in Table 1.[7] The performance of a thermometer is also characterized by another

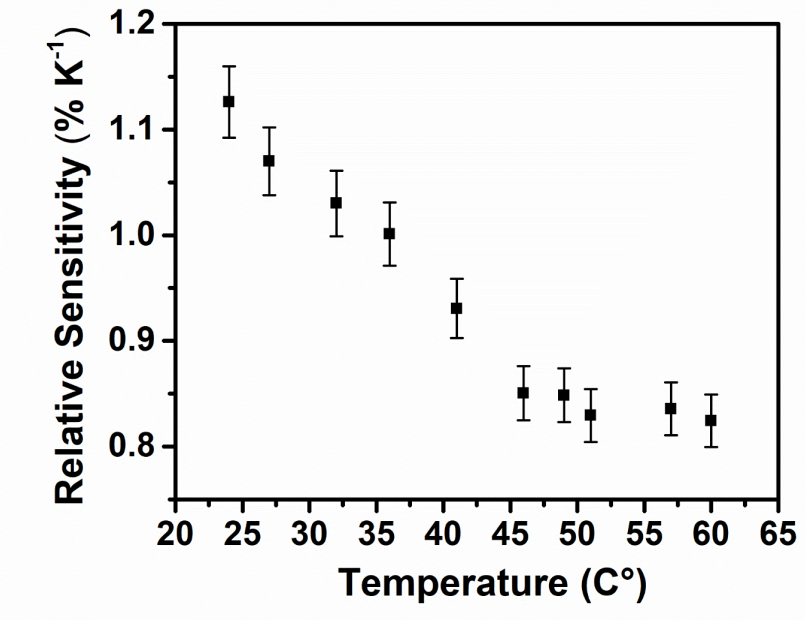

Figure 5 Relative sensitivity of water colloidal dispersions of the SrF_2:Yb^{3+}, Tm^{3+}, Eu^{3+} UCNPs (1 wt %) as a function of temperature.

important parameter, that is the minimum temperature uncertainty, ΔT_{min}, which determines the accuracy of the temperature measurement that can be achieved under the working conditions of the thermometers [4], defined as:

$$\Delta T_{min} = \frac{\Delta LIR}{LIR \cdot S_r} \qquad (3)$$

where ΔLIR represent the experimental uncertainty of the LIR. The average value of ΔT_{min} is evaluated to be 1.9±0.2 °C. It is important to mention that the uncertainty parameter ΔLIR depends on the instrumental setup of the experiments through the signal to noise ratio, and thus it can be improved with longer integration time, higher laser excitation or better detection equipment.

This value is consistent with those found for similar upconverting thermometers[46]. In order to better understand the physical mechanism governing the behavior of the upconversion emission as a function of the temperature, the SrF_2:Yb^{3+},Tm^{3+},Eu^{3+} UCNPs were dispersed in D_2O as the solvent, at a concentration of 1 wt%, similar to the one used for experiments with H_2O as the solvent. These dispersions turned out to be colloidally stable for some weeks.

Host	**Dopants**	**Average particle size (nm)**	**Excitation wavelength (nm)**	**Emission range (nm)**	**S_r @ 25 ºC (% K^{-1})**	**Ref**
ZnO	Er^{3+}	80	978	535-555	0.5	[42]
$NaYF_4$	Er^{3+}, Yb^{3+}	6000	980	530-555	1.2	[43]
$NaY(WO_4)_2$	Er^{3+}, Yb^{3+}	3000	980	530-550	1.0	[44]
$LiNbO_3$	Er^{3+}, Yb^{3+}	100	980	525-550	0.7	[45]
CaF_2	Er^{3+}, Yb^{3+}	11	920	522-538	1.9	[46]
$GdVO_4$	Er^{3+}, Yb^{3+}	3.9	980	525-555	1.1	[47]
$LiLaP_4O_{12}$	Eu^{3+}, Tm^{3+}, Yb^{3+}	40	975	450-700	0.34	[27]
SrF_2	Eu^{3+}, Tm^{3+}, Yb^{3+}	17	980	585-590	1.1	This work

Table 1 Relative sensitivity values for upconversion nanothermometers, based on the luminescence intensity ratiometric (LIR) technique.

It is worth mentioning that the vibrational energy cutoff for D_2O molecule is 2500 cm^{-1}, value than is much less than for the H_2O molecule (highest vibrational energy around 3600 cm^{-1}) [48]

For this reason, multiphonon relaxation processes for lanthanide ions are much more probable if they are close to H_2O molecules than for D_2O ones, as the higher the vibrational energy is, the larger is the multiphonon relaxation probability of the Ln^{3+} excited level. We show in Figure 6a the comparison between upconversion spectra for the $SrF_2:Yb^{3+},Tm^{3+},Eu^{3+}$ UCNPs using H_2O and D_2O as dispersing solvents, while using identical experimental conditions, as the geometrical setup and in particular the same power density of the laser excitation radiation. From Figure 6a, it can be noted that in the case of D_2O dispersions, the Eu^{3+} upconversion bands corresponding to transitions starting from the $^5D_1$ level are more intense than for those starting from the $^5D_0$ one. The upconversion spectra for D_2O dispersions as a function of the temperature (20-60 °C) do not change notably on increasing the temperature (see Figure 6b), suggesting that the populations of the $^5D_0$ and $^5D_1$ levels of the Eu^{3+} ions do not change significantly with the temperature, at least in the investigated range. The LIR for the D_2O dispersed UCNPs shows an almost constant value (around 1.0), within the experimental uncertainties, on increasing the temperature (Figure 6b). Such behavior indicates that the relaxation channel for the $^5D_1$ level is much more effective in H_2O dispersions than

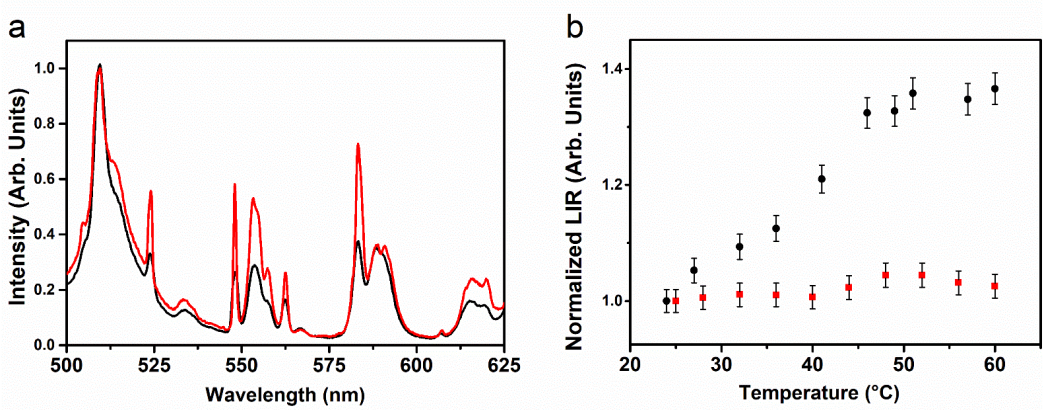

Figure 6 (a) Eu^{3+} upconversion for $SrF_2:Yb^{3+},Tm^{3+},Eu^{3+}$ UCNPs dispersed in H_2O (black line) and in D_2O (red line). (b) LIR for H_2O (black squares) and D_2O (red solid circles) dispersed UCNPs.

in D_2O ones. This behavior is a clear evidence that a significant amount of Ln^{3+} ions lies on the nanoparticle surface, close to the solvent molecules, as their emission properties are much influenced by the solvent vibrational energies, inducing non-radiative multiphonon relaxation channels. The depopulation of the $^5D_1$ energy level of Eu^{3+} is much more influenced by multiphonon relaxations than the $^5D_0$ one, due to much lower energy gap with the lower lying energy level ($^5D_1$ - $^5D_0$, energy gap around 1800 cm^{-1}, $^5D_0$ - $^7F_6$, energy gap around 12000 cm^{-1}). Therefore, the multiphonon relaxation probability for the $^5D_1$ level is almost constant in the relatively small investigated temperature range for D_2O dispersions, while it results to increase for H_2O dispersions, due to much higher vibrational energy of H_2O with respect to D_2O.

The obtained thermometric values for the SrF_2:Yb^{3+},Tm^{3+},Eu^{3+} UCNPs demonstrate that the strategy applied to excite the Eu^{3+} ions offers good opportunities for thermometry in three aspects. First, a careful selection of Ln^{3+} dopants allows to engineer a mechanism that exploits upconversion to excite Eu^{3+} ions. Second, the different upconversion paths used to excite several Eu^{3+} states allow the definition of a luminescence intensity ratio that remains unaffected during measurements, also for variations of the laser excitation power. Finally, the thermal sensitivity of such intensity ratio is on par with the best upconversion nanothermometers reported to date.

4. Conclusions

In the present chapter, we investigated colloidal upconversion nanothermometers based on Yb^{3+}, Tm^{3+} and Eu^{3+} ions that exploits the matching of the Tm^{3+} ions energy levels with the ones of Eu^{3+} ions. This property permits to transfer the absorbed energy by the antenna Yb^{3+} ions to the final probe, Eu^{3+} ions. The developed nanothermometer shows a very good relative sensitivity, around 1 $\%K^{-1}$ in the 20-60 °C range, among the highest values shown by the most popular lanthanide-based nanothermometers. Moreover, the relative sensitivity is independent on intensity fluctuations of the excitation radiation owing to the characteristics of the designed upconversion process. Very importantly, this excitation strategy constitutes a new way of engineering upconversion-based nanothermometers that exploit new ions and that are able to operate at different wavelengths.

5. Bibliografy

1. Aigouy, L., Tessier, G., Mortier, M. & Charlot, B. Scanning thermal imaging of microelectronic circuits with a fluorescent nanoprobe. *Appl. Phys. Lett.* **87,** 184105 (2005).
2. Benayas, A. *et al.* Nd:YAG Near-infrared Luminescent Nanothermometers. *Adv. Opt. Mater.* **3,** 687–694 (2015).
3. del Rosal, B., Ximendes, E., Rocha, U. & Jaque, D. In Vivo Luminescence Nanothermometry: from Materials to Applications. *Advanced Optical Materials* **5,** 1600508 (2017).
4. Jaque, D. & Vetrone, F. Luminescence nanothermometry. *Nanoscale* **4,** 4301–4326 (2012).
5. Brites, C. D. S. *et al.* Thermometry at the nanoscale. *Nanoscale* **4,** 4799–4829 (2012).
6. Wang, X., Wolfbeis, O. S. & Meier, R. J. Luminescent probes and sensors for temperature. *Chem. Soc. Rev.* **42,** 7834–7869 (2013).
7. González-Béjar, M. & Pérez-Prieto, J. Upconversion luminescent nanoparticles in physical sensing and in monitoring physical processes in biological samples. *Methods Appl. Fluoresc.* **3,** 42002 (2015).
8. Auzel, F. Upconversion and anti-stokes processes with f and d ions in solids. *Chem. Rev. (Washington, D. C.)* **104,** 139–173 (2004).
9. Bünzli, J.-C. G. & Eliseeva, S. V. Intriguing aspects of lanthanide luminescence. *Chem. Sci.* **4,** 1939–1949 (2013).
10. Ang, L. Y., Lim, M. E., Ong, L. C. & Zhang, Y. Applications of upconversion nanoparticles in imaging, detection and therapy. *Nanomedicine Nanotechnology, Biol. Med.* **6,** 1273–1288 (2011).
11. Sedlmeier, A., Achatz, D. E., Fischer, L. F., Gorris, H. H. & Wolfbeis, O. S. Photon upconverting nanoparticles for luminescent sensing of temperature. *Nanoscale* **4,** 7090–7096 (2012).
12. Boruc, Z., Kaczkan, M., Fetlinski, B., Turczynski, S. & Malinowski, M. Blue emissions in Dy^3+ doped Y_4Al_2O_9 crystals for temperature sensing. *Opt. Lett.* **37,** 5214 (2012).
13. Cao, Z. *et al.* Temperature dependent luminescence of Dy3+ doped BaYF5 nanoparticles for optical thermometry. *Curr. Appl. Phys.* **14,** 1067–1071 (2014).
14. Nikolić, M. G., Jovanović, D. J. & Dramićanin, M. D. Temperature dependence of emission and lifetime in Eu^3+- and Dy^3+-doped GdVO_4. *Appl. Opt.* **52,** 1716

(2013).

15. Rocha, J., Brites, C. D. S. & Carlos, L. D. Lanthanide Organic Framework Luminescent Thermometers. *Chemistry - A European Journal* **22,** 14782–14795 (2016).
16. Brites, C. D. S. *et al.* Thermometry at the nanoscale using lanthanide-containing organic-inorganic hybrid materials. in *Journal of Luminescence* **133,** 230–232 (2013).
17. Gao, Y. *et al.* A Novel Optical Thermometry Strategy Based on Diverse Thermal Response from Two Intervalence Charge Transfer States. *Adv. Funct. Mater.* **26,** 3139–3145 (2016).
18. Tang, W. *et al.* Ultrahigh-sensitive optical temperature sensing based on ferroelectric Pr3+-doped (K0.5Na0.5)NbO3. *Appl. Phys. Lett.* **108,** 61902 (2016).
19. Rai, V. K. Temperature sensors and optical sensors. *Appl. Phys. B* **88,** 297–303 (2007).
20. Syamchand, S. S. & Sony, G. Europium enabled luminescent nanoparticles for biomedical applications. *J. Lumin.* **165,** 190–215 (2015).
21. Andres, J., Hersch, R. D., Moser, J. E. & Chauvin, A. S. A new anti-counterfeiting feature relying on invisible luminescent full color images printed with lanthanide-based inks. *Adv. Funct. Mater.* **24,** 5029–5036 (2014).
22. Zheng, S. H. *et al.* Lanthanide-doped NaGdF4 core-shell nanoparticles for non-contact self-referencing temperature sensors. *Nanoscale* **6,** 5675–5679 (2014).
23. Martín-Rodríguez, R. *et al.* Upconversion luminescence in nanocrystals of Gd3Ga 5O12 and Y3Al5O12 doped with Tb3+-Yb3+and eu3+-Yb3+. *J. Phys. Chem. C* **113,** 12195–12200 (2009).
24. Jubera, V. *et al.* Yb3+ and Yb3+-Eu3+ luminescent properties of the Li2Lu5O4(BO3)3 phase. *J. Lumin.* **124,** 10–14 (2007).
25. Strek, W., Deren, P. J., Bednarkiewicz, A., Kalisky, Y. & Boulanger, P. Efficient up-conversion in KYb0.8Eu0.2 (WO4)2 crystal. *J. Alloys Compd.* **300,** 180–183 (2000).
26. Dieke, G. H. *Spectra and energy levels of rare-earth ions in crystals*. (Wiley, 1968). doi:10.1119/1.1976350
27. Marciniak, L., Bednarkiewicz, A. & Strek, W. Tuning of the up-conversion emission and sensitivity of luminescent thermometer in LiLaP4O12:Tm,Yb nanocrystals via Eu3+dopants. *J. Lumin.* **184,** 179–184 (2017).
28. Quintanilla, M., Cantarelli, I. X., Pedroni, M., Speghini, A. & Vetrone, F. Intense

ultraviolet upconversion in water dispersible SrF 2 :Tm 3+ ,Yb 3+ nanoparticles: the effect of the environment on light emissions. *J. Mater. Chem. C* **3,** 3108–3113 (2015).

29. Pedroni, M. *et al.* Water (H2O and D2O) Dispersible NIR-to-NIR Upconverting Yb3+/Tm3+ Doped MF2 (M = Ca, Sr) Colloids: Influence of the Host Crystal. *Cryst. Growth Des.* **13,** 4906–4913 (2013).
30. Ostermayer, F. W., Van der Ziel, J. P., Marcos, H. M., Van Uitert, L. G. & Geusic, J. E. Frequency upconversion in YF3-Yb3+, Tm3+. *Phys. Rev. B* **3,** 2698- (1971).
31. Quintanilla, M., Nuñez, N., Cantelar, E., Ocaña, M. & Cusso, F. Tuning from blue to magenta the up-converted emissions of YF3:Tm3+/Yb3+ nanocrystals. *Nanoscale* **3,** 1046–1052 (2011).
32. Hewes, R. A. & Sarver, J. F. Infrared excitation processes for the visible luminescence of Er3+, Ho3+, and Tm3+ in Yb3+-sensitized rare-earth trifluorides. *Phys. Rev. B Condens. Matter* **182,** 427–436 (1969).
33. Jouart, J. P., Bissieux, C., Mary, G. & Egee, M. A spectroscopic study of Eu3+ centres in SrF2 using a site-selective excitation technique. *J. Phys. C Solid State Phys.* **18,** 1539 (1985).
34. Li, Y., Guo, J., Liu, X., Aidilibike, T. & Qin, W. White upconversion luminescence in CaF2:Yb(3+)/Eu(3+) powders via the incorporation of Y(3+) ions. *Phys. Chem. Chem. Phys.* **18,** 16094–16097 (2016).
35. Wang, H. S., Duan, C. K. & Tanner, P. a. Visible Upconversion Luminescence from Y2O3:Eu3+,Yb3+. *J. Phys. Chem. C* **112,** 16651–16654 (2008).
36. MacIel, G. S., Biswas, A. & Prasad, P. N. Infrared-to-visible Eu3+energy upconversion due to cooperative energy transfer from an Yb3+ion pair in a sol-gel processed multi-component silica glass. *Opt. Commun.* **178,** 65–69 (2000).
37. Wang, L. *et al.* Ultraviolet and violet upconversion fluorescence of Europium (III) doped in YF3 nanocrystals. *Opt. Lett.* **34,** 2781–2783 (2009).
38. Lin, H. *et al.* Ultraviolet upconversion luminescence of Gd3+ and Eu3+ in nano-structured glass ceramics. *Mater. Res. Bull.* **47,** 469–472 (2012).
39. Pedroni, M. *et al.* Water (H2O and D2O) Dispersible NIR-to-NIR Upconverting Yb3+/Tm3+ Doped MF2 (M = Ca, Sr) Colloids: Influence of the Host Crystal. *Cryst. Growth Des.* **13,** 4906–4913 (2013).
40. Tanabe, S., Yoshii, S., Hirao, K. & Soga, N. Upconversion properties, multiphonon relaxation, and local environment of rare-earth ions in fluorophosphate glasses. *Phys. Rev. B* **45,** 4620–4625 (1992).

41. Cortelletti, P. *et al.* Luminescence of Eu3+Activated CaF2and SrF2Nanoparticles: Effect of the Particle Size and Codoping with Alkaline Ions. *Cryst. Growth Des.* **18,** 686–694 (2018).
42. Blake, D. M. *et al.* Application of the photocatalytic chemistry of titanium dioxide to disinfection and the killing of cancer cells. *Sep. Purif. Methods* **28,** 1–50 (1999).
43. Zhou, S. *et al.* Upconversion luminescence of NaYF4: Yb3+, Er3+ for temperature sensing. *Opt. Commun.* **291,** 138–142 (2013).
44. Zheng, H. *et al.* Microwave-assisted hydrothermal synthesis and temperature sensing application of Er3+/Yb3+ doped NaY(WO4)2 microstructures. *J. Colloid Interface Sci.* **420,** 27–34 (2014).
45. Quintanilla, M., Cantelar, E., Cusso, F., Villegas, M. & Caballero, A. C. Temperature Sensing with Up-Converting Submicron-Sized LiNbO3:Er3+/Yb3+ Particles. *Appl. Phys. Express* **4,** 22601 (2011).
46. Dong, N. N. *et al.* NIR-to-NIR two-photon excited CaF2:Tm3+,Yb3+nanoparticles: Multifunctional nanoprobes for highly penetrating fluorescence bio-imaging. *ACS Nano* **5,** 8665–8671 (2011).
47. Gavrilović, T. V., Jovanović, D. J., Lojpur, V. & Dramićanin, M. D. Multifunctional Eu3+- and Er3+/Yb3+-doped GdVO4nanoparticles synthesized by reverse micelle method. *Sci. Rep.* **4,** 1–9 (2014).
48. Lappi, S. E., Smith, B. & Franzen, S. Infrared spectra of H216O, H218O and D2O in the liquid phase by single-pass attenuated total internal reflection spectroscopy. *Spectrochim. Acta - Part A Mol. Biomol. Spectrosc.* **60,** 2611–2619 (2004).

Chapter 2

Nd^{3+} activated KY_3F_{10} nanoparticles as nanothermometers based on thermal populated excited state stimulation

1. Introduction

Temperature is a fundamental physical quantity, the measure of which is of great interest in many scientific and technological fields. Most of the sensors used nowadays need direct contact to properly measure the temperature, therefore they are ineffective for sub-micrometric measurements needed in fields of nanomedicine or in the semiconductor industry. Otherwise measurement of temperature distribution is currently performed by narrow-band semiconductor or microbolometric cameras.[1] Such cameras work in the NIR infrared range (wavelength of 3-14 μm) and quantify the temperature by the measure of the black body emission. These cameras have the disadvantages of relatively high cost due to the detector and the optical components and to be not suitable for high spatial resolution or for microscope or fiber based biomedical imaging. In order to solve these problems great effort have been spent to develop temperature dependent photoluminescent materials, such as polymers, proteins, quantum dots, complexes, phosphors, whose emission properties (e.g. luminescence intensity or lifetime) are related with local temperature.[2,3] Luminescent nanoparticles are promising candidates because of their typical photostability, narrow band emission and absorption, and possible surface functionalization.[4] Great efforts have been spent in the recent years to develop nanoparticles with efficient luminescence in the NIR biological windows, suitable for thermometry in nanomedicine.[5] Unfortunately, the luminescence of nanoparticles is usually relatively low and the temperature readout is technically complicated: the temperature dependent parameter is usually connected with small difference in band shape or the spectral band are overlapping and for that the measurement requires high-

resolution monochromators and high brightness of the emission in order to trustworthy convert the temperature dependent parameter in a proper temperature units.

Recently, a new type of optical ratiometric thermometer have been proposed, based on absorption from thermally excited levels. Two different systems have been studied so far: the first was proposed by Souza et al.[6], it is based on Eu^{3+} doped material and the ratiometric thermal parameter is defined as the ratio between the emission intensities of the $^5D_0 \rightarrow {}^7F_4$ transition, when the $^5D_0$ emitting level is populated from the $^7F_0$ ground state and when is excited from the $^7F_1$ or $^7F_2$ thermally excited levels. The second one, proposed by Bednarkiewicz et al.[7,8], is based on Cr^{3+} doped materials with emission around 700 nm. This latter case is focused on a single emission band that varies its emission intensity under two excitation radiations at different energies, in resonant and non-resonant conditions. These systems are based on the different population between two energy levels. According to Boltzmann distribution, the ratio of the relative populations of the excited level (n_1) and the ground state (n_0), is:[9]

$$\frac{n_1}{n_0} = exp\left(-\frac{\Delta E}{k_b T}\right)$$

Where ΔE is the energy difference between the two levels, k_b is the Boltzmann constant and T is the absolute temperature.

These innovative optical thermometers have several advantages compared to the others proposed in the literature. Since they work with two well separated excitation radiations monitoring a single emission, it is not necessary a high-resolution monochromator to measure the temperature, but even filters with relatively large optical bandwidths can be successfully used, even for the excitation radiation, not necessarily to be a laser. Moreover, the simple model behind the thermal excited level population allows an accurate prediction of the properties of the thermometer, following the Boltzmann distribution.

In this work we study the possibility of use the Stark levels of lanthanide doped nanoparticles as thermally excited levels for this kind of thermometer. Specifically,

we exploit the thermometric property of Nd^{3+} doped nanoparticles of KY_3F_{10} excited from the ground level and from an excited Stark level. This system has the interesting characteristic that both excitations and emission radiations can be chosen to be in the biological window.[10] Indeed, the two excitation radiations have been chosen as follows: the first in resonance with the $^4I_{9/2}(Z_1) \rightarrow {}^4F_{5/2}$ transition, and the second at lower energy, in resonance with a $^4I_{9/2}(Z_{exc}) \rightarrow {}^4F_{5/2}$ transition (where Z_1 and Z_{exc} denote the lower Stark level and an excited energy level of the ground state), monitoring the emission at 875 nm. Moreover, we were interested in the study of the upconversion emission of at 450 nm due to the $^1D_2 \rightarrow {}^3F_4$ transition of the Tm^{3+} ions in order to check the thermal performance due to a multistep absorption typical of upconversion process. KY_3F_{10} has been chosen as host because of its high luminescence efficiency for Tm^{3+} upconversion emission sensitized by Nd^{3+} and Yb^{3+} ions[11] and for the well-known energy level Stark structure[12]. In order to improve the upconversion efficiency, a core@shell@shell structure (c@s@s) has been adopted,[13] with a core doped with 3% of Nd^{3+} ions and 10% of Yb^{3+} ions and a shell doped with 0.5% of Tm^{3+} ions and 20% of Yb^{3+} ions (KYF@KYF@KYF). This core@shell structure permits to spatially separate Tm^{3+} ions from Nd^{3+} ones and partially avoid the backtransfer from Tm^{3+} ions to Nd^{3+} ions. A third undoped shell has been added to shield the lanthanide ions from the solvent molecules and minimize non-radiative deexcitation of their excited energy levels and therefore increasing the emission efficiency[14].

2. Experimental

2.1 Nanoparticles Preparation

KY_3F_{10} nanoparticle were synthesized by a hydrothermal reaction method.[15] In a 50 mL Teflon vessel Stochiometric quantity of $YCl_3 \cdot 3H_2O$ and $NdCl_3 \cdot 3H_2O$ and $YbCl_3 \cdot 3H_2O$ (Aldrich 99.99%) (total metal amount of $3.5*10^{-3}$ mole, nominal molar metal ratios Y:Yb:Nd = 87:10:3) were dissolved in 25 mL of water. Then 0.02 moles of potassium citrate (Fluka > 99%) were added and stirred until a homogeneous solution was obtained. 2.5 mL of a solution 3.5 M of NH_4F (Aldrich, 99.9%)

was added drop by drop and the resultant clear solution was heated at 190° under autogenous pressure for 3 hours. After washing with acetone, the nanoparticles were dispersed in deionized water. In order to synthesize the core@shell structure, the same procedure was followed adding 400 mg of the previous prepared core nanoparticles in the starting solution containing the metal precursors. The nominal molar metal ratios of the first shell is Y:Yb:Tm = 89.5:10:0.5 while the last shell is not doped (Y 100%)

2.2 Experimental setup

2.2.1 Structural and morphological investigation

X-ray power diffraction (XRPD) measurements were carried out with a Thermo ARL X'TRA powder diffractometer equipped with a Cu-anode X-ray source with a Peltier Si(Li) cooled solid state detector. Before the measurements, the samples were homogenized in a mortar with few drops of ethanol. After evaporation of the ethanol, the sample was deposited on a low background sample stage.

The transition electron microscope (TEM) images were recorded with a Philips Morgagni TEM, operating at 80kV of voltage. The powders were dispersed in water in order to be deposited on Holey-Carbon Copper grids.

2.2.2 Spectroscopy measurements

Emission spectra were measured using a $Al_2O_3:Ti^{3+}$ laser pumped by the Second Harmonic (532 nm) of a Pulsed Nd:YAG laser System LS-2137 / 2M as exciting source and a Jobin-Yvon THR1000 monochromator with Hamamatsu photomultipliers (R928, R406). The temperature of the sample was controlled using a THMS600 heating stage from Linkam (0.1 °C temperature stability and 0.1 °C set point resolution).

3. Results and discussion

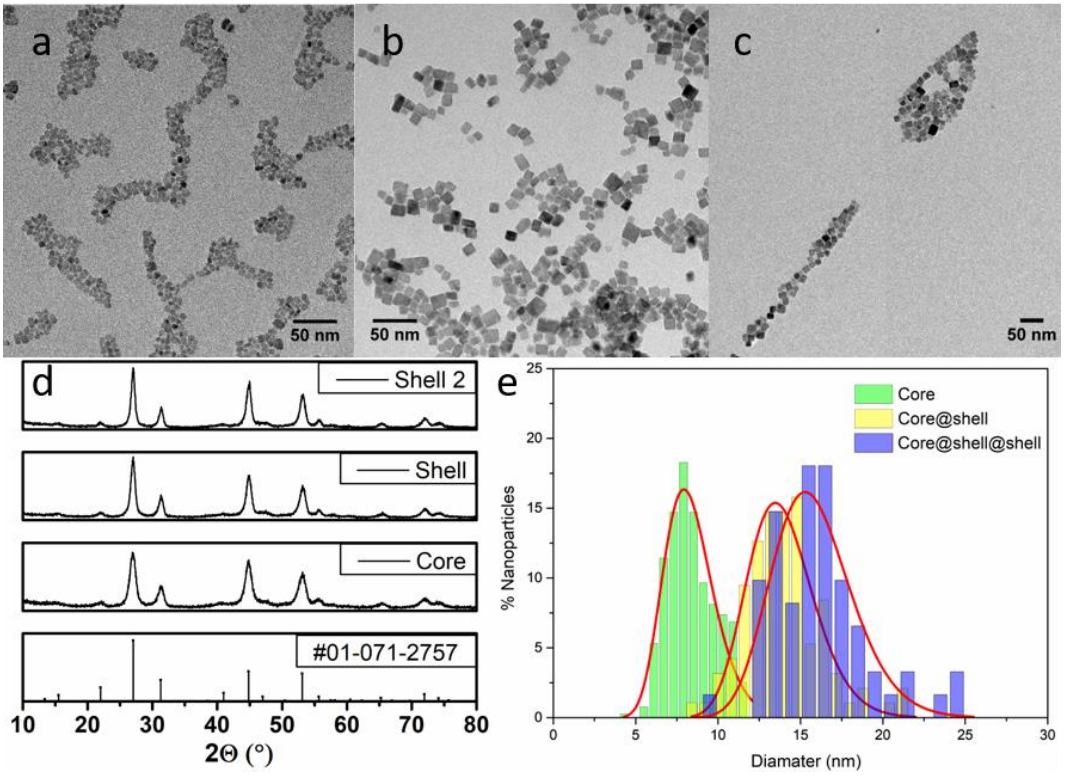

Figure 1 Representative TEM image of (a) core (b) core@shell and (c) c@s@s KY_3F_{10} nanoparticles. (d) XRPD patterns of KY_3F_{10} nanoparticles. (e) Particle size distribution of calculated using Pebbles software and Log-normal fit (average core size: 8 ± 1 nm, core@shell: 14 ± 2 nm, core@shell@shell: 16 ± 2 nm).

XRD measurements in figure 1d show that the all the core and core@shell structures have the same expected cubic structure. Representative TEM images shown in figure 1a, 1b and 1c that the increase in size of the nanoparticle from the core to the core@shell and c@s@s structures (figure 1e).

3.1 Stokes emission

Figure 2a shows the Stokes emission when Nd^{3+} ions are excited at 802 nm ($^4I_{9/2} \rightarrow {}^4F_{5/2}$ transition). The luminescence spectra exhibit three features, around 875 nm and 1060 nm, due to Nd^{3+} ions ($^4F_{3/2} \rightarrow {}^4I_{9/2}$ and $^4F_{3/2} \rightarrow {}^4I_{11/2}$ transitions) and around 1000 nm, due to the Yb^{3+} ions ($^2F_{5/2} \rightarrow {}^2F_{7/2}$ transition).

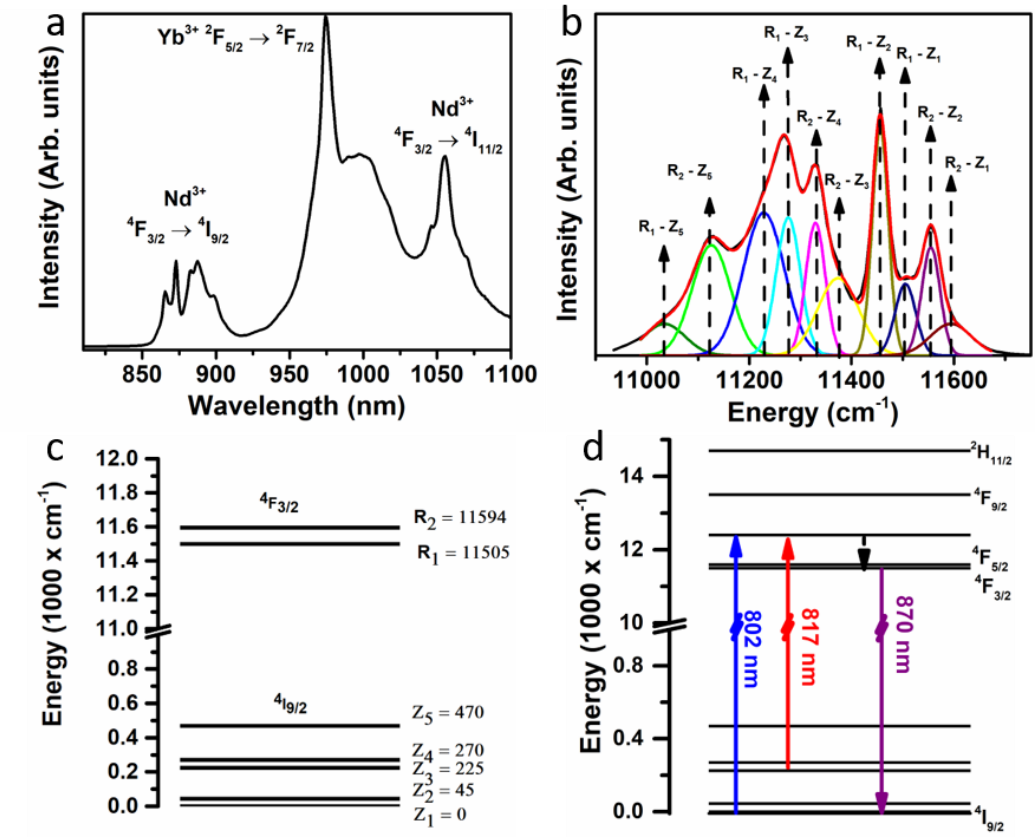

Figure 2 (a) NIR emission spectra of c@s@s nanoparticles with laser excitation at 802 nm at 210 K. (b) Fit of the emission due to the $^4F_{3/2} \rightarrow {}^4I_{9/2}$ transition with gaussian profiles. The emission transitions have been labeled according to (c) the energy level diagram. (d) Energy level scheme with proposed transitions involved in the thermometry.

From a fit procedure of the shape of the Nd^{3+} emission profile at 875 nm (due to $^4F_{3/2} \rightarrow {}^4I_{9/2}$ transitions) it is possible to identify the Stark levels of both $^4F_{3/2}$ and $^4I_{9/2}$ manifolds[16]. To this aim, we deconvolved this spectrum into 10 gaussian components (figure 2b), according to the number of transitions expected to occur considering the two Stark levels of the emitting $^4F_{3/2}$ multiplet and the five components of the $^4I_{9/2}$ ground state. From the fit, an energy level scheme for the doped KY_3F_{10} nanoparticle has been obtained (Figure 2c), compatible to those reported for different Nd^{3+} sites in slightly doped (0.1 mol%) KY_3F_{10} nanoparticles[12]. In this investigation reported in the literature, the excitation spectrum for the $^4I_{9/2} \rightarrow {}^4F_{5/2}$ transition show a broad band in the 770-820 nm range, although a strong narrow band is clearly visible at 802 nm. This band, occurring around the middle of the excitation

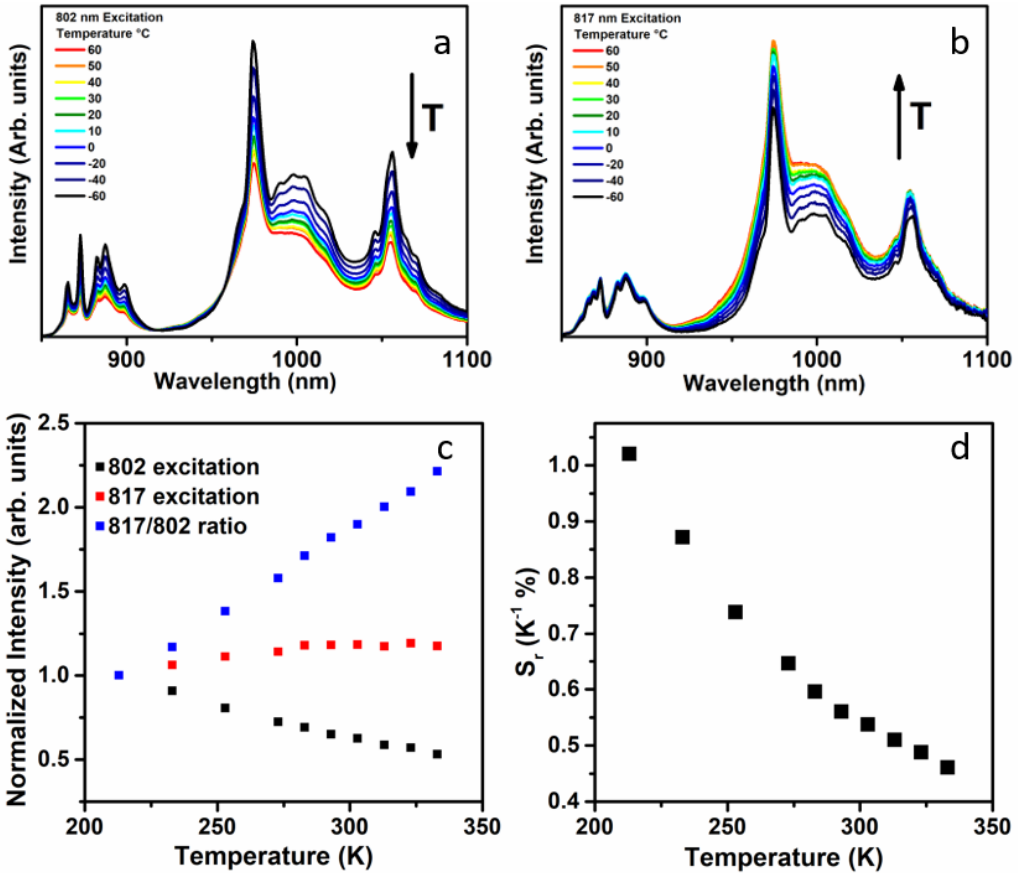

Figure 3 NIR emission spectra of c@s@s nanoparticles as a function of temperature with (a) 802 nm laser excitation and (b) 817 nm laser excitation. (c) Normalized integration of the emission pick around 875 nm as a function of temperature with 802 nm excitation (black dots) and 817 nm excitation (red dots) and normalized thermometric parameter (blue dots). (d) Relative sensitivity of c@s@s NIR emission.

band, could be assigned to a transition starting from the $^4I_{9/2}(Z_1)$ ground state. Transition at lower energies can be considered to start from an excited level of the Stark multiplet of the $^4I_{9/2}$ ground state. Therefore, we focused on the band at lower energy around 817 nm, that we speculate originating from the $^4I_{9/2}(Z_3)$ level, at an energy 225 cm^{-1} higher with respect to the $^4I_{9/2}(Z_1)$ ground state, close enough to have a significant population with respect to the ground state at room temperature. This in our case should be confirmed by further measurements of the excitation spectrum as a function of the temperature. In any case, in order to investigate this aspect, we measured the Stokes emissions by exciting the sample at 802 nm and 817 nm, respectively, as a function the temperature (from -60° to 60°) and they are

shown in Figure 3a and 3b. For excitation at 802 nm, the total emission of the $^4F_{3/2} \rightarrow {}^4I_{9/2}$ transition (around 875 nm) shows a reduction of approximately 53% on varying the temperature. On the other hand, for excitation at 817 nm the total emission of the $^4F_{3/2} \rightarrow {}^4I_{9/2}$ transition shows an increment around 18% (Figure 3c) in the same temperature range, compatible with an increasing population of an excited Stark level of the $^4I_{9/2}$ ground state.

While the increment or decrement of a single transition in a complex matrix as in a biological tissue can be caused by several changes in the experimental conditions, as concentration changes of the emitting particles, the ratiometric technique (exploiting the ratio between two bands in different optical ranges) normalize the calibration curve with respect to several possible interferences.[17] The thermometric parameter in this case can be defined as the ratio between the integrated emission of the $^4F_{3/2} \rightarrow {}^4I_{9/2}$ transition when the $^4F_{5/2}$ level is excited through the excited Stark level of the $^4I_{9/2}$ ground state ($I_{\lambda exc=817}$) and the integrated emission of the same transition when the $^4F_{5/2}$ level is excited from the lower Stark level of the ground state ($I_{\lambda exc=802}$) (figure 3c):

$$R_1 = \frac{I_{\lambda_{exc=817}}}{I_{\lambda_{exc=802}}}$$

In order to compare performance of different thermometers a parameter used in literature is the relative sensitivity S_r:[2]

$$S_r = \frac{1}{R}\left|\frac{dR}{dT}\right|$$

The S_r for the Stokes emission in the core@shell@shell structure is shows in the figure 3d. The maximum relative sensitivity is found at the lowest temperature (-60 °C), of 1.0% K^{-1}, while at physiological temperatures (35 - 40 °C) it results to be 0.5% K^{-1}.

3.2 Upconversion

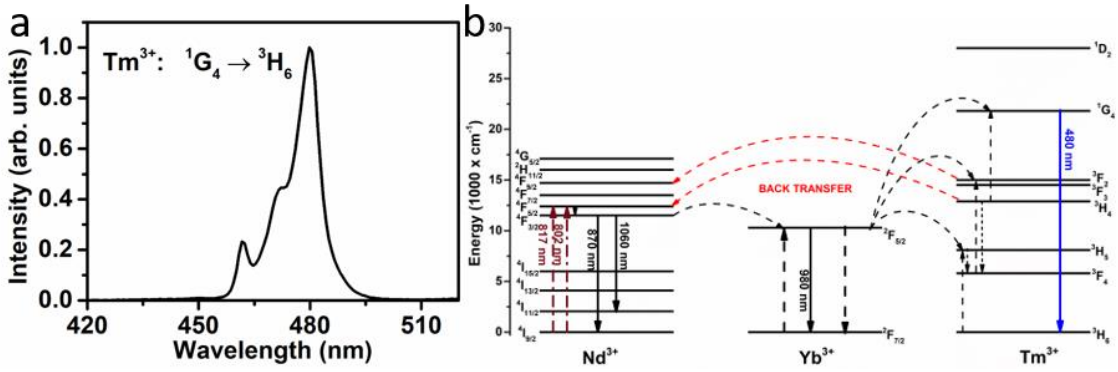

Figure 4 (a) Upconversion blue emission of c@s@s nanoparticles with laser excitation at 802 nm. (b)Energy level scheme and proposed mechanism of upconversion.

Figure 4a shows the upconversion emission of Tm^{3+} around 475 nm ($^1G_4 \rightarrow {}^3H_6$ transition) exciting at 802 nm at room temperature. Figure 4b shows the proposed mechanism of upconversion emission.[18] The absorption of at least three photons are involved in the upconversion emission from $^1G_4$ level. Because of that if the upconversion emission is excited from a thermally populated Stark level, a higher change in the intensity with temperature is expected, and therefore a higher thermal sensitivity.

To explore this point, we studied the temperature influence on the upconversion emission exciting at 802 nm and 817 nm (figure 5a and figure 5b, respectively). For excitation at 802 nm, the $^1G_4 \rightarrow {}^3H_6$ emission band around 475 nm of the Tm^{3+} ions reduces approximately 6% in the investigated temperature range, while for excitation at 817 nm the same upconversion band shows a very large increment of more than 370% (figure 5c).

The S_r of the thermometer based on the upconversion emission is, as expected, improved compared with the one based on the Stokes emission (figure 5d). The maximum S_r is found to be 2.4% per Kelvin at the lowest temperature studied, while it is 0.7% per Kelvin in the physiological range.

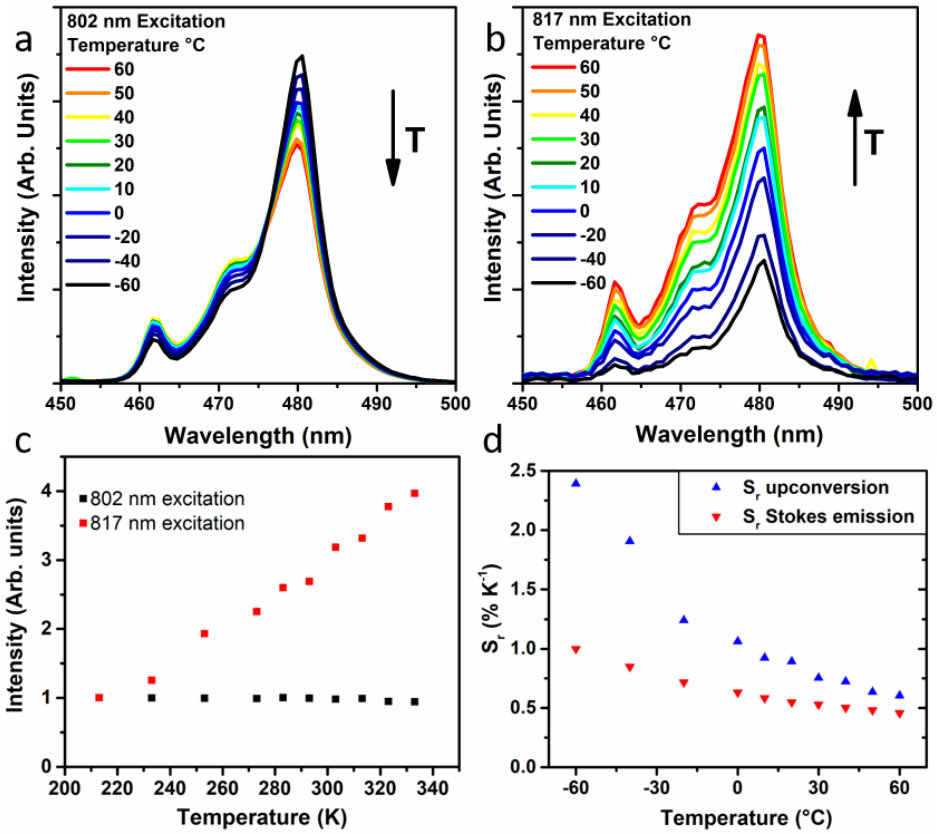

Figure 5 Upconversion emission spectra of c@s@s nanoparticles as a function of temperature with (a) 802 nm laser excitation and (b) 817 nm laser excitation. (c) Normalized integration of the blue upconversion at 480 nm as a function of temperature with 802 nm excitation (black squares) and 817 nm excitation (red squares). (d) Comparison between the relative sensitivity of c@s@s of blue upconversion (blue triangles) and NIR emission (red triangles).

4. Conclusion and perspective

In this chapter, we investigated the optical thermometric property of lanthanide doped nanoparticles exploiting an excitation strategy based on different Stark energy levels of the ground state of the Nd^{3+} ions in the KY_3F_{10} host. The peculiar emissions of Nd^{3+} ions allow the development of a nanothermometer with both excitation and emission located in the NIR biological window with a sensitivity of 0.5 % C^{-1} in the physiological range. This methodology allows to measure the temperature using a cheap, filter-based system for collecting the signal. Moreover, a core@shell@shell nanoparticle structure has been successful synthesized to investigate the thermometric properties based on the upconversion of Tm^{3+} ions sensitized by Nd^{3+} or Yb^{3+} ions. This is the first upconversion nanothermometer based on non-resonant excitation and pave the way on the development of similar system with higher sensitivity.

5. Bibliography

1. Kim, M. M. *et al.* Microscale thermometry: A review. *Microelectron. Eng.* **148,** 129–142 (2015).
2. Jaque, D. & Vetrone, F. Luminescence nanothermometry. *Nanoscale* **4,** 4301–4326 (2012).
3. Quintanilla, M. & Liz-Marzán, L. M. Guiding Rules for Selecting a Nanothermometer. *Nano Today* **19,** 126–145 (2018).
4. Ang, L. Y., Lim, M. E., Ong, L. C. & Zhang, Y. Applications of upconversion nanoparticles in imaging, detection and therapy. *Nanomedicine Nanotechnology, Biol. Med.* **6,** 1273–1288 (2011).
5. del Rosal, B., Ximendes, E., Rocha, U. & Jaque, D. In Vivo Luminescence Nanothermometry: from Materials to Applications. *Advanced Optical Materials* **5,** 1600508 (2017).
6. Souza, A. S. *et al.* Highly-sensitive Eu $^{3+}$ ratiometric thermometers based on excited state absorption with predictable calibration. *Nanoscale* **8,** 5327–5333 (2016).
7. Bednarkiewicz, A., Trejgis, K., Drabik, J., Kowalczyk, A. & Marciniak, L. Phosphor-Assisted Temperature Sensing and Imaging Using Resonant and Nonresonant Photoexcitation Scheme. *ACS Appl. Mater. Interfaces* acsami.7b13649 (2017). doi:10.1021/acsami.7b13649
8. Morassuti, C. Y., Nunes, L. A. O., Lima, S. M. & Andrade, L. H. C. Eu^{3+}-doped alumino-phosphate glass for ratiometric thermometer based on the excited state absorption. *J. Lumin.* 0–1 (2017). doi:10.1016/j.jlumin.2017.09.001
9. Saïdi, E. *et al.* Scanning thermal imaging by near-field fluorescence spectroscopy. *Nanotechnology* **20,** (2009).
10. Pansare, V. J., Hejazi, S., Faenza, W. J. & Prud'Homme, R. K. Review of long-wavelength optical and NIR imaging materials: Contrast agents, fluorophores, and multifunctional nano carriers. *Chem. Mater.* **24,** 812–827 (2012).
11. Silva, H. M. *et al.* Synthesis and characterization of KY 3 F 10 :Yb:Nd:Tm crystals. *J. Phys. Conf. Ser* **249,** (2010).
12. Orlovskii, Y. V. *et al.* NIR fluorescence quenching by OH acceptors in the Nd3+ doped KY3F10 nanoparticles synthesized by microwave-hydrothermal treatment. *J. Alloys Compd.* **661,** 312–321 (2016).
13. Wang, F. *et al.* Tuning upconversion through energy migration in core-shell nanoparticles. *Nat. Mater.* **10,** 968–973 (2011).
14. Chan, E. M., Levy, E. S. & Cohen, B. E. Rationally Designed Energy Transfer in Upconverting Nanoparticles. *Adv. Mater.* **27,** 5753–5761 (2015).

15. Pedroni, M. *et al.* Water (H2O and D2O) Dispersible NIR-to-NIR Upconverting Yb3+/Tm3+ Doped MF2 (M = Ca, Sr) Colloids: Influence of the Host Crystal. *Cryst. Growth Des.* **13,** 4906–4913 (2013).

16. Rocha, U. *et al.* Subtissue thermal sensing based on neodymium-doped LaF3nanoparticles. *ACS Nano* **7,** 1188–1199 (2013).

17. Quintanilla, M. & Liz-Marzán, L. M. Guiding Rules for Selecting a Nanothermometer. *Nano Today* **19,** 126–145 (2018).

18. Baek, S. & Epureanu, B. Reduced Order Modeling of Bladed Disks With Friction Ring Dampers. *Vol. 7A Struct. Dyn.* **249,** V07AT32A028 (2016).

Chapter 3
Broadband Cr^{3+} sensitization for Yb^{3+} emission

1. Introduction

Lanthanide doped UC systems are able to emit ultraviolet (UV), visible or near infrared (NIR) luminescence when excited in the NIR range, through multiple absorption of photons with lower energy.[1] The possibility of this multiple absorption, as mentioned above, is due to the long lifetimes of the electronic excited levels and the ladder-like energy level scheme of the lanthanide ions. UCNPs have many advantages over other luminescent particles, such as organic dyes, fluorescent protein and quantum dots, such as a narrow and non-blinking emission, and high photostability and large anti-Stokes shifts. These properties make them promising for many applications both in biological areas (nanothermometry, bio-sensing, drug delivery, photodynamic therapy or theranostic) and in the technological one (solar cells and displays).

One of the limits that still restricts the practical application of UC nanoparticles is their relatively low brightness, that is intrinsically connected with the low absorption cross section of lanthanide ions. In order to improve the emission efficiency, different strategies have been adopted, such as considering a core/shell architecture of the nanoparticles (active core and inert shell or active core and active shell with optimized lanthanide concentrations)[2], tailoring the best crystal structure of the host[3,4] or coupling the nanoparticles with plasmonic structures to have plasmonic enhancement[5]. All these methods allowed an enhancement of upconversion by one to three orders of magnitude. On the other hand, the weak NIR absorption of lanthanide ions was still a problem, with low photon harvesting capability. Usually the UC process is based on the absorption of NIR radiation by Yb^{3+} ions (usually defined as sensitizers) and the multiple nonradiative energy transfer to other lanthanide ions such us Er^{3+}, Ho^{3+} or Tm^{3+} (activators) that can emit visible or ultraviolet luminescence. But the Yb^{3+} ions absorb the radiation in an optical spectral range around 980 nm with a small absorption cross-section compared with the ones of

organic dyes or transition metal ions.[6] This fundamental limitation prevents UCNPs to harvest efficiently NIR radiation, in order to generate bright upconversion.

In recent years a new method has been exploited to sensitize upconversion luminescence using organic dyes as antennae in order to harvest a much larger part of photons in the NIR range.[7,8] It has been shown that dye antennae can enhance the upconversion luminescence brightness by more than 3 order of magnitude, thanks to the much larger absorption cross section of organic dyes compared with that of lanthanide ions. But the organic dyes have a much lower photo-, thermal- and chemical- stability that are one of the main advantages of the use of lanthanide nanoparticles. Taking inspiration from these studies we tried to develop a new way to sensitize lanthanide ions using transition metal ions doped inorganic nanoparticles. Indeed, transition metal (TM) ions share with organic dyes a broad and more intense absorption cross section than lanthanide ions. In fact, TM ions are commonly used for infrared tunable lasers:[9] the most used materials for infrared tunable lasers are Ti^{3+} doped Sapphire ($Al_2O_3:Ti^{3+}$), Cr^{3+} doped complex fluorides (as $LiSrAlF_6:Cr^{3+}$ or $LiCaAlF_6:Cr^{3+}$)[10] and Cr^{3+} doped monoclinic tungstate or molybdate ($MgWO_4:Cr^{3+}$,[11] $ZnWO_4:Cr^{3+}$ or $MgMoO_4:Cr^{3+}$).[12]

Al_2O_3 is not very suitable as host for lanthanide doping because the Al^{3+} ion is much smaller than lanthanide ions, making lanthanide substitution difficult. For this reason, we focused our attention in hosts as $NaSrAlF_6:Cr^{3+}$, Yb^{3+} and $ZnWO_4:Cr^{3+}$, Yb^{3+}.

2. Experimental

2.1 Nanoparticles preparation

2.1.1 $NaSrAlF_6$ nanoparticles synthesis

$NaSrAlF_6$:Cr^{3+}, Yb^{3+} nanoparticles were synthesized by a hydrothermal reaction with a microwave reactor (Monowave 400, Anton Paar). In a 30 mL glass vessel stochiometric quantity of $AlCl_3 \cdot 6H_2O$ (99%) (Alfa Aesar), $SrCl_2 \cdot 6H_2O$ (99.0%), NaCl (99%), $CrCl_3 \cdot 6H_2O$ (99%) and $YbCl_3 \cdot 6H_2O$ (99.99%) (Sigma Aldrich) (total metal amount of $7.5*10^{-4}$ mol) were dissolved in 10 mL of water. The nominal molar ratios of the metals were Na:Sr:Al:Cr:Yb =1:0.95:0.99:0.01:0.05. 2.3 mL of a solution 3.5 M of NH_4F (Fluka > 99%) was added drop by drop and the resultant pale green suspension was heated at 200° under autogenous pressure for 30 minutes. After washing with acetone, the nanoparticles were dispersed in deionized water. The nanoparticles were then dried at 80° overnight for further characterization.

2.1.2 $ZnWO_4$ nanoparticles synthesis

$ZnWO_4$ nanoparticles were synthesized by a hydrothermal reaction.[13] In a 50 mL Teflon vessel stochiometric quantity (nominal metal molar ratio Zn::Cr:Yb:W = 0.949:0.01:0.05:1) of $ZnCl_2 \cdot 6H_2O$ (> 99% Sigma Aldrich) and $CrCl_3 \cdot 6H_2O$ and $YbCl_3 \cdot 6H_2O$ (total metal amount of $2.5*10^{-3}$ mole) were dissolved in 15 mL of water. Then 10 mL of a solution 0.25 M of Na_2WO_4 (99% Alfa Aesar) was added drop by drop and the resultant white suspension was heated at 190° under autogenous pressure for 12 hours. After washing with acetone, the nanoparticles were dispersed in deionized water.

According to the literature a shell growth can be prepared[14] with: 0.2 mol of previous prepared nanoparticles were added into a flask with 40 mL of water and refluxed continuously. Then 0.9 mL of $ZnCl_2$ 0.02M, 0.1 mL of $YbCl_3$ 0.02M and 1mL of Na_2WO_4 0.02M (nominal metal molar ratio Zn:W:Yb = 0.9:1:0.1) were added and solution was kept refluxing for 3 hours. The addition of the precursors of the shell was repeated 3 times and the last time 0.02 mL of $ErCl_3$ 0.02 M were added. The solution was then left cooling naturally and the nanoparticles collected

with centrifugation. The nanoparticles were then dry at 80° overnight for further characterization.

2.2 Experimental setup

2.2.1 Structural and morphological investigation

X-ray power diffraction (XRPD) measurements were carried out with a Thermo ARL X'TRA powder diffractometer equipped with a Cu-anode X-ray source with a Peltier Si(Li) cooled solid state detector. Before the measurements, the samples were homogenized in a mortar with few drops of ethanol. After evaporation of the ethanol, the sample was deposited on a low background sample stage.

The transition electron microscope (TEM) images were recorded with a Philips Morgagni TEM, operating at 80kV of voltage, equipped with Mega-View G3 CCD camera. The powders were dispersed in water in order to be deposited on Holey-Carbon Copper grids.

2.2.2 Spectroscopy measurements

Emission and excitation spectra were recorded on powders with a modular spectrofluorometer (Nanolog/Fluorolog-3-2iHR320, Horiba-Jobin Yvon, spectral resolution of 1 nm) equipped with Xenon lamp (450W, ozone free) completed of current-stabilized power supplies.

3. Results and discussion

3.1 $NaSrAlF_6:Cr^{3+}$, Yb^{3+}doped nanoparticles

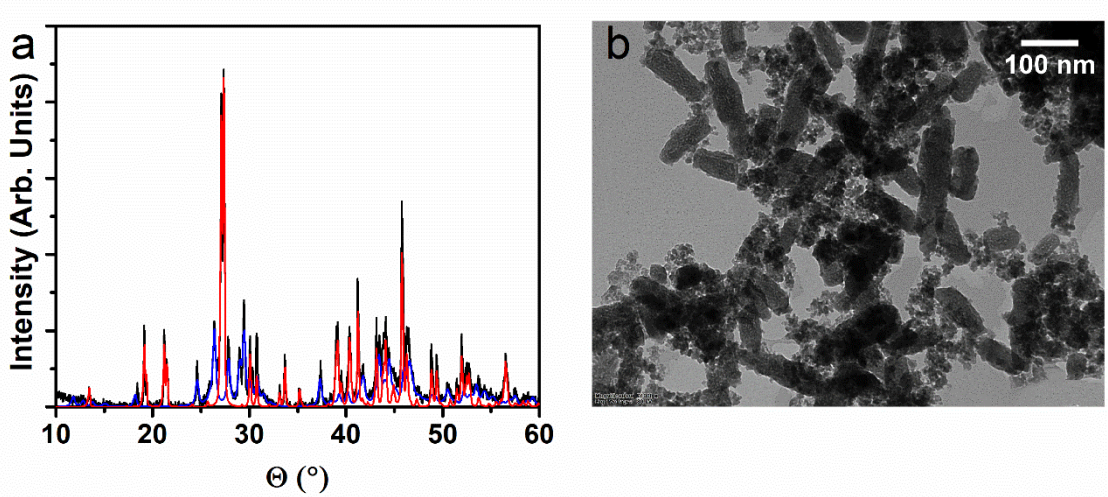

Figure 1 a) XRPD pattern of $NaSrAlF_6:Cr^{3+}$, Yb^{3+} nanoparticles (black line). Rietveld refinement, using MAUD software with $NaSrAlF_6$ phase (red line) and $SrAlF_5$ phase (blue line). b) Representative TEM images for $NaSrAlF_6:Cr^{3+}$, Yb^{3+} nanoparticles.

XRPD measurements show the presence of two crystalline phases: a predominant phase of $NaSrAlF_6$ and another minority phase of $SrAlF_5$ (Figure 1a). The XRPD data were fit with Maud software using the orthorhombic phase of $NaSrAlF_6$ (ICSD 69433) of *Pna2₁* space group and the tetragonal phase of $SrAlF_6$ (ICSD 50474) of *I41/a* space group. The fit parameters show an increment of the *c* cell parameter of $NaSrAlF_6$ of 0.1% while the *a* and *b* cell parameters have a slight decrease of 0.02 and 0.05% respectively. The *a* cell parameter of $SrAlF_6$ has an increment of 2% while the *b* cell parameter decreases of 0.8%. The average particle size for the predominant and the minority phase is 175 nm and 35 nm, respectively. The Cr^{3+} ions is most probably substituting preferentially the Al^{3+} ones because of the similarity of the ionic radii (ionic radius Cr^{3+}: 61pm six-fold coordination[15]; ionic radius Al^{3+}: 54 pm six-fold coordination[15]) while the Yb^{3+} ions substitute preferentially the Sr^{2+} ones (ionic radius Yb^{3+} : 87 pm, Sr^{2+} : 118 pm).[15]

The morphology of the $NaSrAlF_6$ nanoparticles were investigated by TEM technique. From the TEM images, two populations of nanoparticles were deduced.

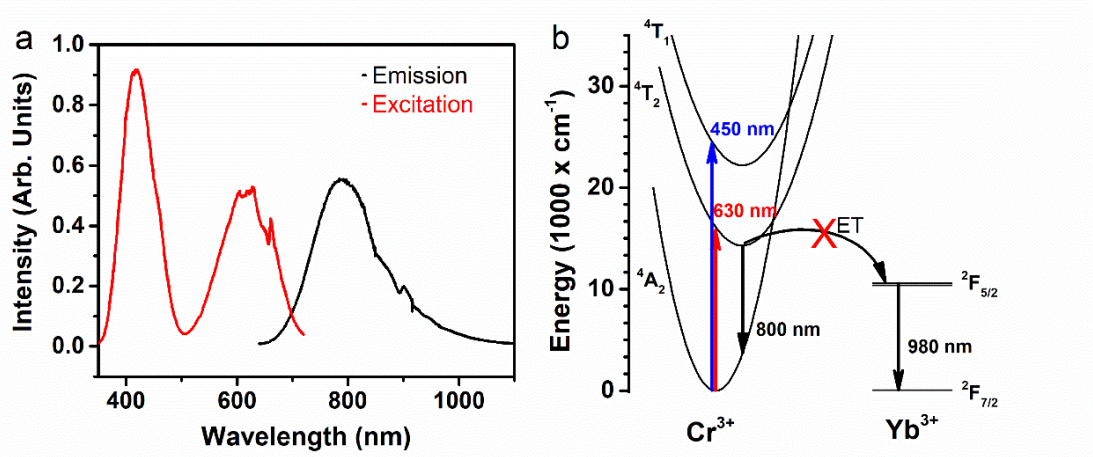

Figure 2 a) Emission (black line) and excitation (red line) of powder sample of $NaSrAlF_6:Cr^{3+}, Yb^{3+}$ doped nanoparticles b) Energy level scheme for Cr^{3+} and Yb^{3+} ions and proposed radiative transitions.

Bigger features are nanorods, with longer size around 200 nm and aspect ratio about 4:1. Other nanoparticles with apparent irregular shape are present, with average size smaller than 30 nm. The morphology analysis is in good agreement with the average particle size obtained from the fit of XRPD data.

The excitation and emission spectra of the $NaSrAlF_6:Cr^{3+}$ doped nanoparticles are shown in figure 2a. A strong and broad infrared emission centered at 790 nm is present, while there are two broad bands of excitation, one centered at 420 nm and one at 620 nm. These features are typical of Cr^{3+} ions in a low crystal field environment (Dq/B>2) such as in other fluoride host as $LiSrAlF_6$ or SrF_2. For these cases, the $^4T_2$ energy state is localized below $^4T_1$ and no emission from ^2E state can be observed. From the excitation and emission spectra is possible to determine the energy diagram of Cr^{3+} and Yb^{3+} (Figure 2b).

Figure 1a) Emission spectra (black line) of $NaSrAlF_6:Cr^{3+}$, Yb^{3+} with excitation at 600 nm and excitation spectra (red line) with emission at 800 nm. b) Energy level diagram of Cr^{3+} and Yb^{3+} ions in $NaSrAlF_6$ with arrows that indicates the principal optical transitions.

Even if there is a partial overlap between the emission of Cr^{3+} ions and the absorption of Yb^{3+} ions in the 950-1000 nm region, no emission of Yb^{3+} ions could be detected. This can be explained by the notable mismatch between the $^4T_2$ energy

level of Cr^{3+} ions and $^2F_{5/2}$ the energy level of Yb^{3+} ones (around 3700 cm-1), that does not allow an efficient Cr^{3+} → Yb^{3+} energy transfer process. In addition, a phonon assisted Cr^{3+} → Yb^{3+} energy transfer has a low probability because of the low phonon energy of the fluoride host and therefore the need for many phonons to fill the energy mismatch. A radiative energy transfer could in principle be possible but most probably because of the low absorption cross section of Yb^{3+} ions it is very unfavored and emission from Yb^{3+} ions are not visible. Therefore, the Cr^{3+} ions are not suitable for an efficient Yb^{3+} sensitization in $NaSrAlF_6$.

3.1 $ZnWO_4:Cr^{3+}$, Yb^{3+} nanoparticles

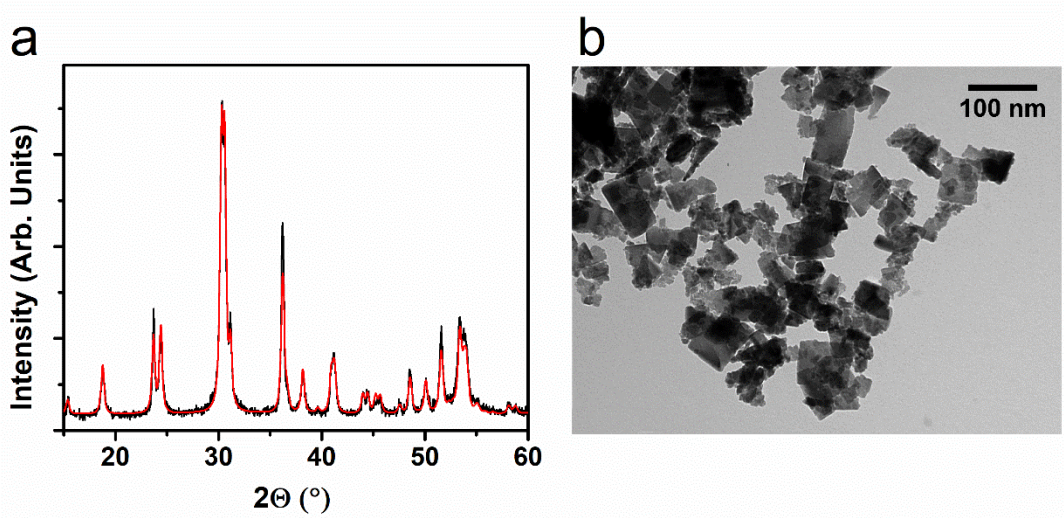

Figure 3 a) XRPD pattern of $ZnWO_4:Cr^{3+}$, Yb^{3+} nanoparticles (black line). Rietveld refinement, using MAUD software (red line). b) Representative TEM images for $ZnWO_4:Cr^{3+}$, Yb^{3+} nanoparticles.

Phase purity of the synthesized nanocrystalline powders was confirmed by XRPD measurements (Figure 3a). The XRPD data were fit with Maud software using the monoclinic phase of $ZnWO_4$ (ICSD 87933) of *P12/c1* space group. Both the Cr^{3+} ions and the Yb^{3+} are most probably substituting the Zn^{2+} ions (ionic radius Zn: 74 pm in a VI fold coordination).[15] No evidence of other phases formation was noted even for dopant concentrations as high as 10%. The fit parameters show an increase of the lattice parameter of less than 0.3%.

The morphology was investigated with TEM analysis (Figure 3b). The nanoparticles show a notable size dispersion, although under 100 nm.

The excitation and emission bands of $ZnWO_4$ nanoparticles doped with 1% of Cr^{3+}

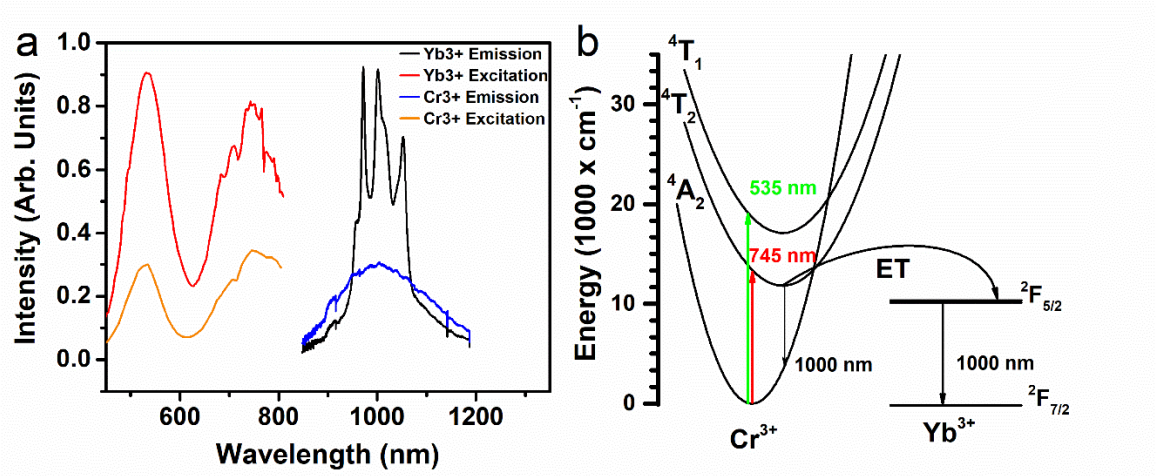

Figure 4 a) Emission (blue line) and excitation (orange line) of powder sample of $ZnWO_4:Cr^{3+}$ nanoparticles and emission (black line) and excitation (red line) of powder sample of $ZnWO_4:Cr^{3+}$, Yb^{3+} nanoparticles. b) Energy level scheme for Cr^{3+} and Yb^{3+} ions and proposed radiative transitions.

ions without Yb^{3+} ions are shown in figure 4a. A weak infrared emission centered at 1000 nm and 2 broad excitation bands at 745 nm and 535 nm are present. The energy diagrams for Cr^{3+} ions in $ZnWO_4$ host and in $NaSrAlF_6$ are similar, although the energy are lower for the latter host, because of the lower crystal field experimented by Cr^{3+} in this environment (Figure 4b). In this case, the $^4T_2$ level of Cr^{3+} is able to sensitize Yb^{3+} ions. Indeed, for $ZnWO_4:Cr^{3+}$, Yb^{3+}, a clear Yb^{3+} emission around 1000 nm is observed, due to its $^2F_{5/2} \rightarrow {}^2F_{7/2}$ transition. The excitation spectrum for this band is typical sensitization by Cr^{3+} ions (Figure 4a).

In order to sensitize Yb^{3+} for UC, the material should be codoped with activator ions such as Er^{3+}, Tm^{3+} or Ho^{3+}. Nonetheless, codoping with Cr^{3+} and activator ions gives rise to a back energy transfer from the excited states of the activator to the excited states of Cr^{3+} and the upconversion luminescence would be strongly quenched (Figure 5).[16] This is why it is possible to have Cr^{3+} upconversion sensitized bulk material only for very low concentration of Cr^{3+} and the activator ions.[16] In order to solve this issue, we thought it would be possible to adopt a core-shell approach for nanoparticles, growing a shell doped with Yb^{3+} and Er^{3+} around a $ZnWO_4:Cr^{3+}$, Yb^{3+} core.[2,14] The synthesized core-shell nanoparticles phase and morphology were studied with XRD and TEM analysis respectively (Figure 6).

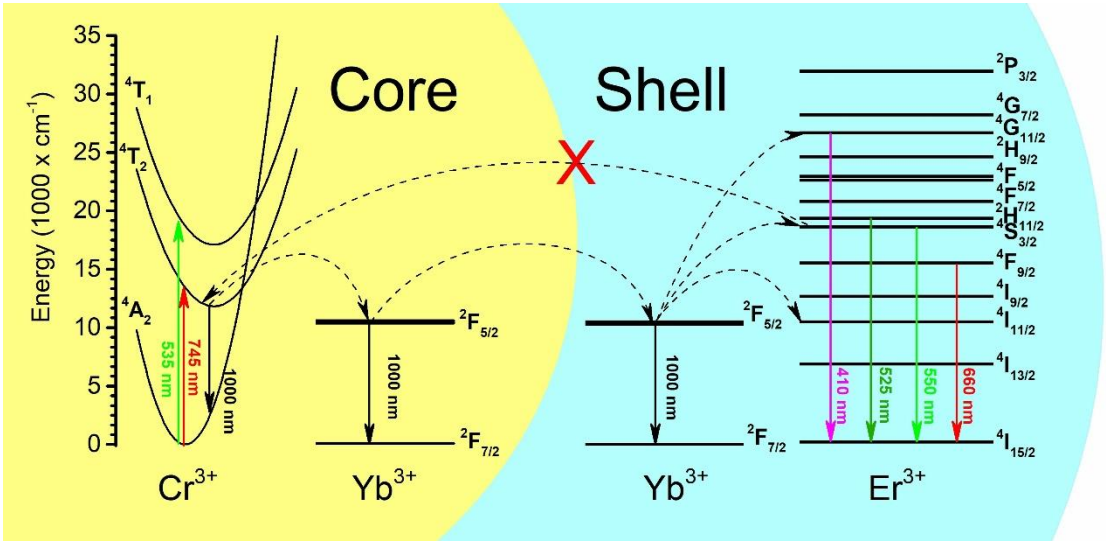

Figure 5 Energy level scheme of $ZnWO_4$ core-shell nanoparticles with the most important transition and energy transfer signed with arrows.

From TEM images, it seems that an irregular shell has grown on the core particles, but because of the high size dispersion of the core nanoparticles it is difficult to properly define the shell thickness.

We measured the upconversion emission with direct excitation of Yb^{3+} ions (980 nm diode laser) to check the effective incorporation of Er^{3+} and Yb^{3+} ions in the $ZnWO_4$ host (figure 7).

In order to study the effective sensitization of Yb^{3+} ions with Cr^{3+} ions, we used a diode laser at 800 nm as excitation source (around 800 mW), but we did not see any

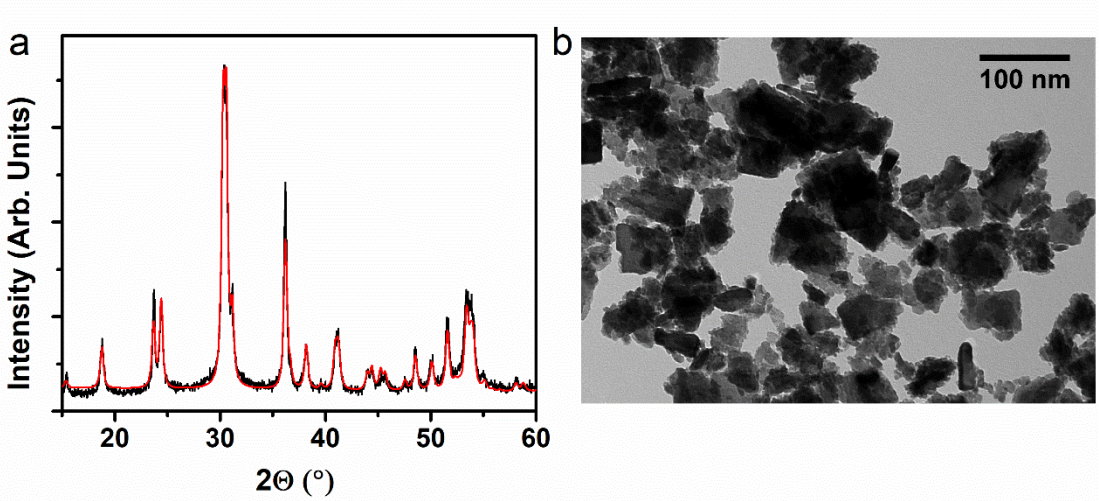

Figure 6 a) XRPD pattern of $ZnWO_4$:Cr^{3+}, Yb^{3+}@Yb^{3+}, Er^{3+} core-shell nanoparticles (black squares). Rietveld refinement, using MAUD software (red line). b) Representative TEM images for $ZnWO_4$ core-shell nanoparticles.

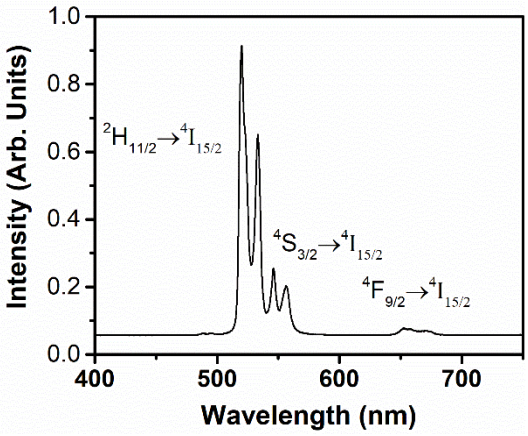

Figure 7 Visible upconversion emission of $ZnWO_4$:Cr^{3+}, Yb^{3+}@Yb^{3+}, Er^{3+} core shell structure with excitation at 980 nm.

upconversion emission and therefore the Cr^{3+} ions do not act as sensitizers with respect to Er^{3+} ions. Therefore, it is not clear at the moment if a shell doped with Yb^{3+} and Er^{3+} ions is formed around the $ZnWO_4$ core or some Yb^{3+} and Er^{3+} doped $ZnWO_4$ nanoparticles are obtained separately. Further studies are needed to improve the synthesis of the core of $ZnWO_4$:Cr^{3+}, Yb^{3+} to have more regular shape and size of the nanoparticles and to grow in a more controlled and reproducible way the core@shell structure.

4. Conclusions and perspectives

In this chapter we studied the possibility to sensitize Yb^{3+} ions with Cr^{3+} ions in order to have a stronger and much broader absorption in the near infrared region. Two different host have been investigated, $NaSrAlF_6$ and $ZnWO_4$, and nanoparticles have been successfully synthesized. The emission and energy transfer between Cr^{3+} ions and Yb^{3+} ions have been characterized. In $NaSrAlF_6:Cr^{3+}$, Yb^{3+} nanoparticles a strong NIR emission from Cr^{3+} ions at around 800 nm has been detected but the $^4A_2$ level of the donor was at too high energy to proper sensitize the $^2F_{5/2}$ state of the acceptor. Instead in $ZnWO_4:Cr^{3+}$, Yb^{3+} nanoparticles a clear sensitization of Yb^{3+} ions by Cr^{3+} ions can be seen from the broad excitation in the visible and infrared region of Yb^{3+}. Nevertheless, future studies are needed in order to have a broad excited upconversion emission because a core@shell structure should be synthesized to have a proper distance between the Cr^{3+} and Er^{3+} ions and avoid a back energy transfer.

5. Bibliography

1. Zhou, J., Liu, Q., Feng, W., Sun, Y. & Li, F. Upconversion luminescent materials: Advances and applications. *Chem. Rev.* **115,** 395–465 (2015).
2. Wang, F. *et al.* Tuning upconversion through energy migration in core-shell nanoparticles. *Nat. Mater.* **10,** 968–973 (2011).
3. Wang, F. *et al.* Simultaneous phase and size control of upconversion nanocrystals through lanthanide doping. *Nature* **463,** 1061–1065 (2010).
4. Dong, H. *et al.* Efficient Tailoring of Upconversion Selectivity by Engineering Local Structure of Lanthanides in Na<inf>x</inf>REF<inf>3+x</inf> Nanocrystals. *J. Am. Chem. Soc.* **137,** 6569–6576 (2015).
5. Schietinger, S., Aichele, T., Wang, H. Q., Nann, T. & Benson, O. Plasmon-enhanced upconversion in single NaYF4:Yb3+/Er3+codoped nanocrystals. *Nano Lett.* **10,** 134–138 (2010).
6. Werts, M. H. V. Making sense of lanthanide luminescence. *Sci. Prog.* **88,** 101–131 (2005).
7. Huang, X. Broadband dye-sensitized upconversion: A promising new platform for future solar upconverter design. *J. Alloys Compd.* **690,** 356–359 (2017).
8. Zou, W., Visser, C., Maduro, J. A., Pshenichnikov, M. S. & Hummelen, J. C. Broadband dye-sensitized upconversion of near-infrared light. *Nat. Photonics* **6,** 560–564 (2012).
9. Jenssen, H. P., Lai, S. T., Lai, S. T. & Materials, E. Tunable-laser characteristics and spectroscopic properties of. **3,** 115–118 (1986).
10. Demirbas, U. *et al.* Low-cost, single-mode diode-pumped Cr:Colquiriite lasers. *Opt. Express* **17,** 1726–1729 (2009).
11. Zhang, L. *et al.* Thermal and spectral characterization of Cr3+:MgWO4- A promising tunable laser material. *J. Lumin.* **169,** 161–164 (2016).
12. Cavalli, E., Belletti, A. & Brik, M. G. Optical spectra and energy levels of the Cr3+ions in MWO4(M=Mg, Zn, Cd) and MgMoO4crystals. *J. Phys. Chem. Solids* **69,** 29–34 (2008).
13. Yu, S. H. *et al.* General synthesis of single-crystal tungstate

nanorods/nanowires: A facile, low-temperature solution approach. *Adv. Funct. Mater.* **13,** 639–647 (2003).

14. Liu, B. *et al.* Nanorod-Direct Oriented Attachment Growth and Promoted Crystallization Processes Evidenced in Case of $ZnWO_4$. *J. Phys. Chem. B* **108,** 2788–2792 (2004).
15. Shannon, R. D. Revised effective ionic radii and systematic studies of interatomic distances in halides and chalcogenides. *Acta Crystallogr. Sect. A* **32,** 751–767 (1976).
16. Ye, S. *et al.* Broadband Cr^3+-sensitized upconversion luminescence in La_3Ga_5GeO_14: Cr^3+,Yb^3+,Er^3+. *Opt. Mater. Express* **4,** 638 (2014).

Conclusions

Lanthanide doped luminescent nanoparticles proved their ability to develop interesting functional properties, exploiting their ladder-like particular energy level structure.

In Chapter 1 a ratiometric thermometer based on Eu^{3+} ion luminescence activated through upconversion processes was proposed. Tridoped SrF_2: Yb^{3+}, Tm^{3+}, Eu^{3+} nanoparticles allow the sensitization in the NIR radiation by Yb^{3+} ions that, through multiple energy transfer to Tm^{3+}, excite the Eu^{3+} ions. The luminescence of the latter shows a thermal relative sensitivity of 1.1% C^{-1} at 25 °C, comparable to the best lanthanide-based thermometer reported to date. The complex design of this nanoparticle is the only way to proper exploit the Eu^{3+} thermal sensible emission, that cannot be achieved with direct UV or NIR excitation.

In Chapter 2 we showed that Nd^{3+} doped nanoparticles can be used as optical thermometers in the first biological window taking advantage of excitation from a thermally excited level. We developed a thermometric parameter based on the ratio between a single emission with two different excitations: one from the ground level and one from a thermally populated excited level. One of the advantages of this system is the possibility to measure the temperature with a simple experimental setup, using a low resolution monochromator or a filters system, since the difference in the emission intensity rely on the excitation source. Moreover, both the excitation and emission energies are in the NIR biological window, therefore suitable for optical bioimaging applications. Besides that, this system can also be used with upconversion emission, showing a higher thermal resolution. These results pave the way to the development of new kinds of upconverting nanothermometers.

In chapter 3 we studied the possibility to sensitize Yb^{3+} ions with Cr^{3+} ions in two different kinds of nanoparticles. Since Cr^{3+} have a broader and stronger absorption cross section compared to Yb^{3+} ions, an enhancement of the upconversion would be expected. We successfully synthesized $NaSrAlF_6$:Cr^{3+}

nanoparticles with strong NIR emission, but the excited energy level of Cr^{3+} ions and Yb^{3+} ions have too high difference in energy for a proper sensitization of Yb^{3+} ions. Therefore, we synthesized $ZnWO_4:Cr^{3+}$, Yb^{3+} nanoparticles that have a redshift in the excitation and emission bands of Cr^{3+} ions with respect to the fluoride based $NaSrAlF_6$ nanoparticles that allow the sensitization of Yb^{3+} ions. Further studies are needed for improve the nanoparticles size distribution and to grow a shell on them in order to spatially separate Cr^{3+} and Er^{3+} ions and avoid a back energy transfer, but the results achieved are promising for the development of a broadband excitation of upconversion emission.

Acknowledgments